NAVAL POSTGRADUATE SCHOOL

MONTEREY, CALIFORNIA

THESIS

INVESTIGATION OF FREQUENCY AGILITY FOR LPI-SAR WAVEFORMS

by

Zachary A. Wagner

December 2018

Thesis Advisor: David A. Garren
Co-Advisor: Phillip E. Pace

Approved for public release. Distribution is unlimited.

THIS PAGE INTENTIONALLY LEFT BLANK

REPORT DOCUMENTATION PAGE	*Form Approved OMB No. 0704-0188*

1. AGENCY USE ONLY ***(Leave blank)***	**2. REPORT DATE** December 2018	**3. REPORT TYPE AND DATES COVERED** Master's thesis

4. TITLE AND SUBTITLE INVESTIGATION OF FREQUENCY AGILITY FOR LPI-SAR WAVEFORMS	**5. FUNDING NUMBERS**
6. AUTHOR(S) Zachary A. Wagner	
7. PERFORMING ORGANIZATION NAME(S) AND ADDRESS(ES) Naval Postgraduate School Monterey, CA 93943-5000	**8. PERFORMING ORGANIZATION REPORT NUMBER**
9. SPONSORING / MONITORING AGENCY NAME(S) AND ADDRESS(ES) N/A	**10. SPONSORING / MONITORING AGENCY REPORT NUMBER**

11. SUPPLEMENTARY NOTES The views expressed in this thesis are those of the author and do not reflect the official policy or position of the Department of Defense or the U.S. Government.

12a. DISTRIBUTION / AVAILABILITY STATEMENT Approved for public release. Distribution is unlimited.	**12b. DISTRIBUTION CODE** A

13. ABSTRACT (maximum 200 words)

This thesis investigates the feasibility of using Costas frequency shift transmission waveforms to generate spotlight Synthetic Aperture Radar (SAR) images. A spotlight SAR image formation algorithm is used to evaluate the radar returns from scenes containing multiple point scatterers. Two-dimensional imagery is used to investigate the sidelobe effects. The peak sidelobe ratio (in dB) is determined from the one-dimensional slices in both the down-range and cross-range dimensions. Three unique Costas frequency shift sequence lengths are used in the investigation, $N = 15$, 100, and 150.

Results of this investigation show that Costas frequency shift sequences are practical for the formation of spotlight SAR images. The autocorrelation sidelobe levels resulting from the Costas waveform are reduced with an increasing sequence length, providing an improved peak-to-sidelobe ratio. Image scenes with multiple neighboring scatterers are interrogated. Results show a spotlight SAR image peak-to-sidelobe ratio of – 20 dB, – 40 dB, and – 44 dB for $N = 15$, 100, and 150, respectively, thus offering the potential for producing high-quality spotlight SAR imagery while maintaining the strategic advantages of low probability of intercept.

14. SUBJECT TERMS synthetic aperture radar, peak side lobe level, Costas sequence, frequency hopping, range sidelobes	**15. NUMBER OF PAGES** 91
	16. PRICE CODE

17. SECURITY CLASSIFICATION OF REPORT Unclassified	**18. SECURITY CLASSIFICATION OF THIS PAGE** Unclassified	**19. SECURITY CLASSIFICATION OF ABSTRACT** Unclassified	**20. LIMITATION OF ABSTRACT** UU

NSN 7540-01-280-5500 Standard Form 298 (Rev. 2-89) Prescribed by ANSI Std. 239-18

THIS PAGE INTENTIONALLY LEFT BLANK

Approved for public release. Distribution is unlimited.

INVESTIGATION OF FREQUENCY AGILITY FOR LPI-SAR WAVEFORMS

Zachary A. Wagner
Civilian, Raytheon
BSEE, California State University - San Jose, 1996

Submitted in partial fulfillment of the
requirements for the degree of

MASTER OF SCIENCE IN ELECTRICAL ENGINEERING

from the

NAVAL POSTGRADUATE SCHOOL
December 2018

Approved by: David A. Garren
Advisor

Phillip E. Pace
Co-Advisor

Clark Robertson
Chair, Department of Electrical and Computer Engineering

THIS PAGE INTENTIONALLY LEFT BLANK

ABSTRACT

This thesis investigates the feasibility of using Costas frequency shift transmission waveforms to generate spotlight Synthetic Aperture Radar (SAR) images. A spotlight SAR image formation algorithm is used to evaluate the radar returns from scenes containing multiple point scatterers. Two-dimensional imagery is used to investigate the sidelobe effects. The peak sidelobe ratio (in dB) is determined from the one-dimensional slices in both the down-range and cross-range dimensions. Three unique Costas frequency shift sequence lengths are used in the investigation, $N = 15$, 100, and 150.

Results of this investigation show that Costas frequency shift sequences are practical for the formation of spotlight SAR images. The autocorrelation sidelobe levels resulting from the Costas waveform are reduced with an increasing sequence length, providing an improved peak-to-sidelobe ratio. Image scenes with multiple neighboring scatterers are interrogated. Results show a spotlight SAR image peak-to-sidelobe ratio of – 20 dB, – 40 dB, and – 44 dB for $N = 15$, 100, and 150, respectively, thus offering the potential for producing high-quality spotlight SAR imagery while maintaining the strategic advantages of low probability of intercept.

THIS PAGE INTENTIONALLY LEFT BLANK

TABLE OF CONTENTS

I. INTRODUCTION 1
- A. SYNTHETIC APERTURE RADAR 1
- B. SAR IMAGING HISTORY 2
- C. COSTAS WAVEFORMS 3
- D. PREVIOUS WORKS 6
- E. RESEARCH OBJECTIVES AND APPROACH 6
- F. THESIS OUTLINE 7

II. TECHNICAL BACKGROUND 9
- A. PRINCIPLES OF SYNTHETIC APERTURE RADAR 9
- B. SPOTLIGHT-MODE DATA COLLECTION 13
- C. SQUINT ANGLE 15
- D. THE RANGE DOPPLER ALGORITHM 15
- E. POLAR-TO-RECTANGULAR CONVERSION 17
- F. PRINCIPLES OF COSTAS-CODED WAVEFORMS 19

III. SIMULATION METHODOLOGY 23
- A. SPOTLIGHT SAR SIMULATION SETUP 24
- B. RANGE PROFILE PLOTS 27
- C. CROSS-RANGE PROFILE PLOTS 28

IV. SIMULATION RESULTS 29
- A. DETAILED SINGLE SCATTERING CENTER ANALYSIS 29
  1. Length-15 Costas Code 29
  2. Length-100 Costas Code 34
  3. Length-150 Costas Code 38
  4. Summary of Length-15, Length-100 and Length-150 Costas Codes for Generating SAR Images of a Single Scattering Center 41
- B. DETAILED MULTIPLE SCATTERING CENTER ANALYSIS 43
  1. Length-15 Costas Code 43
  2. Length-100 Costas Code 48
  3. Length-150 Costas Code 52

V. CONCLUSIONS AND RECOMMENDATIONS 57
- A. SUMMARY AND CONCLUSIONS 57
- B. FUTURE WORK 58

APPENDIX A. SPECIFIC CODES USED IN THE SIMULATIONS 59

APPENDIX B. CRITICAL MATLAB CODE SEGMENTS......................................63
A. FUNCTION TO GENERATE A COSTAS WAVEFORM 63
B. CODE SNIPPET TO PROCESS THE WAVEFORM RESPONSE AGAINST THE SCATTERING CENTERS 67

LIST OF REFERENCES..69

INITIAL DISTRIBUTION LIST 71

LIST OF FIGURES

Figure 1. Forming an Image with a Radar Requires a Narrow Beam for Fine Cross-Range Resolution. Adapted from [1]..2

Figure 2. The Matched Filtering Process 5

Figure 3. The Ambiguity Function of a Length-25 Costas Code 5

Figure 4. Image Formation Using the Real Aperture Imaging System.....................10

Figure 5. Two Primary Modes of SAR Are Spotlight SAR (above) and Strip Map SAR (below). Adapted from [2]. 12

Figure 6. Pulse Collection in Strip-Map SAR. Adapted from [2]. 13

Figure 7. Forward and Back Squint in Strip-Map SAR. Adapted from [2]. 16

Figure 8. Block Diagram of the Range Doppler Algorithm.....................................17

Figure 9. Conversion of Polar Samples to Keystone Samples. Adapted from [2]. 18

Figure 10. Sampling of Keystone Samples onto the Final Rectangular Grid. Adapted from [2]..19

Figure 11. A Six-Sequence Costas-Coded Pulse...20

Figure 12. A Binary Time-Frequency Matrix for Costas Sequence {1,2,5,4,6,3}......21

Figure 13. Time and Frequency Coincidence of a Six-Sequence Costas Code 22

Figure 14. Example of a Ground Range Profile...27

Figure 15. Example of a Ground Cross-Range Profile 28

Figure 16. Length-15 Costas Code SAR Image of a Single Scattering Center Using the Parameters Defined in Table 1, Row One 30

Figure 17. Length-15 Costas Code SAR Image Range Profile Slice of a Single Scattering Center Using the Parameters Defined in Table 1, Row One 30

Figure 18. Length-15 Costas Code SAR Image Cross-Range Profile Slice of a Single Scattering Center Using the Parameters Defined in Table 1, Row One 31

Figure 19. Overlay of Five Unique Length-15 Costas Code SAR Image Range Profile Slices of a Single Scattering Center Using the Parameters Defined in Table 1, Rows 1–5 32

Figure 20. SAR Images of a Single Scattering Center Resulting from Five Unique Length-15 Costas Codes Using the Parameters Defined in Table 1, Rows 1–5 33

Figure 21. Length-100 Costas Code SAR Image of a Single Scattering Center Using the Parameters Defined in Table 1, Row 6....................34

Figure 22. Length-100 Costas Code SAR Image Range Profile Slice of a Single Scattering Center Using the Parameters Defined in Table 1, Row 6.........35

Figure 23. Length-100 Costas Code SAR Image Range Profile Slice of a Single Scattering Center Using the Parameters Defined in Table 1, Row 6.........36

Figure 24. Overlay of Five Unique Length-100 Costas Code SAR Image Range Profile Slices for a Single Scattering Center Using the Parameters Defined in Table 1, Rows 6–10 36

Figure 25. SAR Images Resulting from Five Unique Length-100 Costas Codes for a Single Scattering Center, as Defined in Table 1, Rows 6–10 37

Figure 26. Length-150 Costas Code SAR Image for a Single Scattering Center Using the Parameters Defined in Table 1, Row 11....................38

Figure 27. Length-150 Costas Code SAR Image Range Profile Slice for a Single Scattering Center Using the Parameters Defined in Table 1, Row 11 39

Figure 28. Length-150 Costas Code SAR Image Cross-Range Profile Slice for a Single Scattering Center Using the Parameters Defined in Table 1, Row 11 39

Figure 29. SAR Images Resulting from Five Unique Length-150 Costas Codes for a Single Scattering Center Using the Parameters Defined in Table 1, Rows 11–15 40

Figure 30. Overlay of Five Unique Length-150 Costas Code SAR Image Range Profile Slices for a Single Scattering Center Using the Parameters Defined in Table 1, Rows 11–15 41

Figure 31. SAR Images Produced by Three Different Length Costas Codes: a Length-15 Costas Code (a), a Length-100 Costas Code (b), and a Length-150 Costas Code (c) 42

Figure 32. Overlay of Three Different Length Costas Code SAR Image Range Profile Slices Corresponding to Lengths of 15, 100, and 150 for a Single Scattering Center Using the Parameters Defined in Table 1, Rows 1, 6 and 11 43

Figure 33. Length-15 Costas Code SAR Image with Multiple Scattering Centers Using the Parameters Defined in Table 1, Row 1 44

Figure 34. Length-15 Costas Code SAR Image Range Profile Slice for Multiple Scattering Centers Using the Parameters Defined in Table 1, Row 1 45

Figure 35. Length-15 Costas Code SAR Image Cross-Range Profile Slice for Multiple Scattering Centers Using the Parameters Defined in Table 1, Row 1 45

Figure 36. Overlay of Five Unique Length-15 Costas Code SAR Image Range Profile Slices for Multiple Scattering Centers Using the Parameters Defined in Table 1, Rows 1–5 46

Figure 37. SAR Images Resulting from Five Unique Length-15 Costas Codes for Multiple Scattering Centers Using the Parameters Defined in Table 1, Rows 1–5 47

Figure 38. Length-100 Costas Code SAR Image with Multiple Scattering Centers Using the Parameters Defined in Table 1, Row 6 48

Figure 39. Length-100 Costas Code SAR Image Range Profile Slice for Multiple Scattering Centers Using the Parameters Defined in Table 1, Row 6 49

Figure 40. Length-100 Costas Code SAR Image Cross-Range Profile Slice for Multiple Scattering Centers Using the Parameters Defined in Table 1, Row 6 49

Figure 41. Overlay of Five Unique Length-100 Costas Code SAR Image Range Profile Slices for Multiple Scattering Centers Using the Parameters Defined in Table 1, Rows 6–10 50

Figure 42. SAR Images of Five Unique Length-100 Costas Codes for Multiple Scattering Centers Using the Parameters Defined in Table 1, Rows 6–10 51

Figure 43. Length-150 Costas Code SAR Image with Multiple Scattering Centers Using the Parameters Defined in Table 1, Row 11 52

Figure 44. Length-150 Costas Code SAR Image Range Profile Slice for Multiple Scattering Centers Using the Parameters Defined in Table 1, Row 11 53

Figure 45. Length-150 Costas Code SAR Image Cross-Range Profile Slice for Multiple Scattering Centers Using the Parameters Defined in Table 1, Row 11 53

Figure 46. Overlay of Five Unique Length-150 Costas Code SAR Image Range Profile Slices for Multiple Scattering Centers Using the Parameters Defined in Table 1, Rows 11–15 54

Figure 47. SAR Images of Five Unique Length-150 Costas Codes for Multiple Scattering Centers Using the Parameters Defined in Table 1, Rows 11–15....................55

LIST OF TABLES

Table 1. List of Waveforms and Parameters 23
Table 2. SAR Simluation Parameters 24
Table 3. Primary Modules Used in the Simulation of SAR Images 25
Table 4. Definition of Scattering Scenes 26

THIS PAGE INTENTIONALLY LEFT BLANK

LIST OF ACRONYMS AND ABBREVIATIONS

1D	One Dimensional
2D	Two Dimensional
FFT	Fast Fourier Transform
FSK	Frequency-Shift Keying
IFFT	Inverse Fast Fourier Transform
ISLR	Integrated Side Lobe Ratio
JPL	Jet Propulsion Laboratory
LPI	Low Probability of Intercept
NASA	National Aeronautics and Space Administration
NOAA	National Oceanic and Atmospheric Administration
PRF	Pulse-Repetition Frequency
PRI	Pulse-Repetition Interval
PSK	Phase-Shift Keying
PSLR	Peak Side Lobe Ratio
RDA	Range Doppler Algorithm
SAR	Synthetic Aperture Radar

THIS PAGE INTENTIONALLY LEFT BLANK

ACKNOWLEDGMENTS

I would like to express my utmost gratitude to my thesis advisor, Professor Garren, for his patience over the past years in encouraging and guiding me through the completion of this thesis. I would also like to thank Professor Pace for providing input and guidance on the development of the thesis.

I would like to thank my wife, Ede, who has supported me through my pursuit of my master's degree from the Naval Postgraduate School. Ede kept two young children occupied for many weekends and nights, providing me windows of concentration. Without her support the completion of this thesis would not have been possible.

Finally, I want to thank Raytheon for providing the time and resources to advance my education.

THIS PAGE INTENTIONALLY LEFT BLANK

I. INTRODUCTION

A. SYNTHETIC APERTURE RADAR

Synthetic Aperture Radar (SAR) imaging utilizes radar signals to generate two-dimensional and three-dimensional images. The advantage of SAR over optical imaging is that is does not require a light source, and it can easily penetrate clouds or foliage which would obscure a target from an optical sensor [1]. SAR imaging can easily generate images with sub-meter resolution. SAR imaging is used extensively in science and military applications. In this introduction, we present an overview of SAR with a brief history of SAR.

Forming an image with a radar requires a narrow beam for fine cross-range resolution. The size of the beam on the ground grows as the range from the platform to the image area increases, making it difficult to use a real-aperture system for imaging. In a radar-imaging system, the ground area illuminated by an antenna is a function of the antenna beamwidth and the distance of the antenna to the region being imaged. The wider the antenna beamwidth or greater the distance between the radar system and the ground, the larger the imaged area as shown in Figure 1 [2]. Reflections off all targets within the illuminated area are returned to the radar system, making it impossible for a real-aperture system to discern individual targets. Detection of individual targets can only be accomplished by improving the resolution of the radar system by reducing the beamwidth. Reducing the beamwidth of a real-aperture system is accomplished by increasing the size of the antenna; however, the goal of obtaining image resolutions in the meter range requires that the size of the antenna to be several kilometers long, which is impossible for most applications which use aircraft or satellites for imaging [2].

The alternative to using a very large real aperture to obtain very fine image resolutions is to use a synthetic aperture. Synthetic Aperture Radar systems provide high resolution imagery through the use of an antenna with a much wider beamwidth.

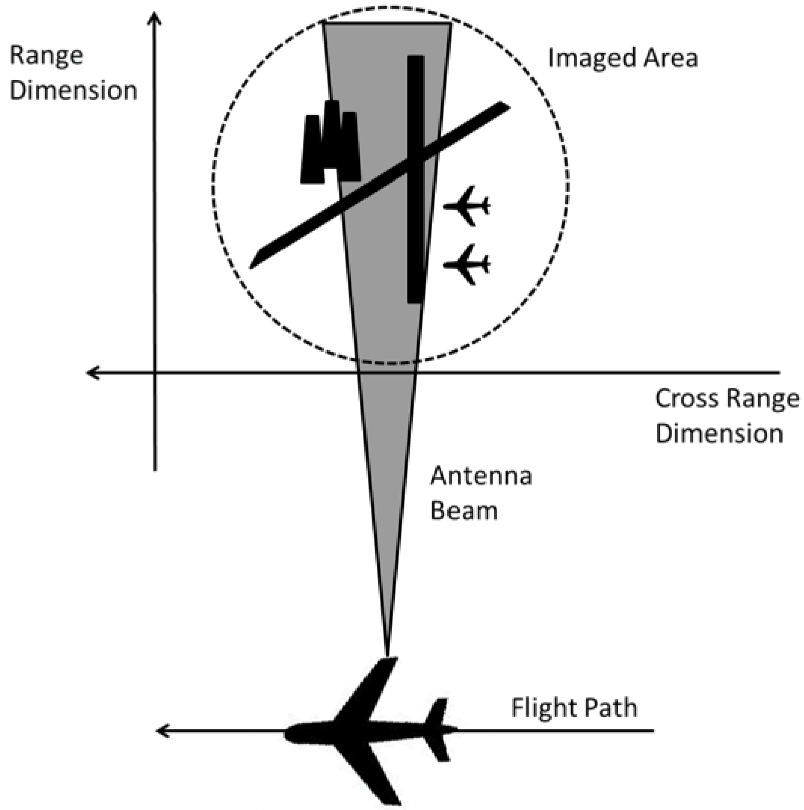

Figure 1. Forming an Image with a Radar Requires a Narrow Beam for Fine Cross-Range Resolution. Adapted from [1].

A synthetic aperture uses a standard-sized real aperture and captures several returns from an area to be imaged as the radar moves past the area. The phase data of each radar return is saved to build a phase history. This phase history is processed through a range-Doppler algorithm to develop an image that is much higher in resolution than is possible using only the real-beam radar data without the range Doppler algorithm processing.

B. SAR IMAGING HISTORY

In the early 1950s, Carl Wiley, working for the Goodyear Corporation, determined that the Doppler shifts of a series of pulses transmitted from a moving real-aperture radar could be analyzed to generate a better along-track resolution [1]. This formed the basis for what is today known as Synthetic Aperture Radar. Development in SAR continued from the 1950s through the 1970s primarily in military and industrial corporations such as

Goodyear, Hughes, and Westinghouse. The first acknowledged SAR system was the U.S. Army AN/UPD-1 mounted in a Beechcraft. The system was developed in the 1960s in coordination with the University of Michigan. This system led to a version fitted onto an F-4 and used in Vietnam and was the beginning of SAR system usage by the military [3].

In the mid-1970s engineers at the Jet Propulsion Laboratory (JPL) joined with National Aeronautics and Space Administration (NASA) engineers and the National Oceanic and Atmospheric Administration (NOAA) engineers to begin work on a new space-based SAR for monitoring the world’s oceans. The result was the first non-military SAR system named SEASAT [4]. SEASAT operated for several months in 1978 until it experienced a critical failure. SEASAT represented a major milestone in the SAR development because it was the first to use digital processing of the phase data to generate images.

Prior SAR systems used data recorded on film with optical processing to analyze the phase data and generate images. To keep the optical systems that performed the Fourier transforms to a manageable size, the data was recorded on 35 mm film; however, at this size the patterns on the film prevented image focusing due to diffraction effects. This limitation drove the desire for a digital approach that was successfully answered by MacDonald Dettwiler (MDA), a Canadian aerospace company, in 1978 [4]. The digital processor developed by MDA was used in SEASAT. The resulting images had much better resolution than the images generated through the optical processing method, but the higher resolution came at the expense of processing time. A few seconds of collected data took several hours of processing to generate an image.

C. COSTAS WAVEFORMS

The selection of waveform for a radar system is very important, and the SAR system is no different. Two key concepts in the selection of the waveform are the waveform bandwidth and the detection range. Bandwidth of the waveform drives the resolution of a radar system. Higher bandwidth waveforms result in better range resolution [5].

The traditional radar generates a pulse of radio frequency (RF) energy and uses the elapsed time between the transmission of the pulse and the reception of received energy reflected off a distant target to determine the distance to the target [1]. A radar that uses a short pulse width (high bandwidth) is able to distinguish two closely spaced targets, whereas a radar with a longer pulse width (lower bandwidth) receives overlapping pulses from the two targets which make it impossible to measure exact range to the trailing target [5]. The range at which the radar is required to operate drives the amount of transmitter power required. From the radar-range equation we can see that the received power from a target decays as the forth power of the range to the target; therefore, the amount of required power increases significantly for a radar pulse to be effective at long ranges [5]. The high transmit power complicates the design of the system. The higher power requires a larger power source, more cooling, more volume, and thus, is more expensive to design, build, and operate. The large transmit power also makes a radar system easier to detect. For military applications where stealth is the ultimate advantage, a high-power radar is not acceptable.

A method for overcoming the high power requirements of traditional radar while also achieving very high bandwidths is through pulse compression waveforms [6]. Pulse compression involves the modulating of a long pulse and then the use of a matched filter on the received pulse. The result of matched filtering is a pulse that is compressed in time but increased in power as shown in Figure 2. A pulse compression waveform results in a high range resolution due to the high bandwidth of the signal, while the pulse compression gain allows for lower transmit power [7].

The two primary methods for modulating a pulse for use in pulse compression are phase modulation and frequency modulation. There are a number of phase modulation schemes: a) binary-phase codes, such as Barker codes, and b) poly-phase codes, such as Frank codes, Tn codes, and Pn codes [8]. Costas codes are a popular frequency modulation scheme.

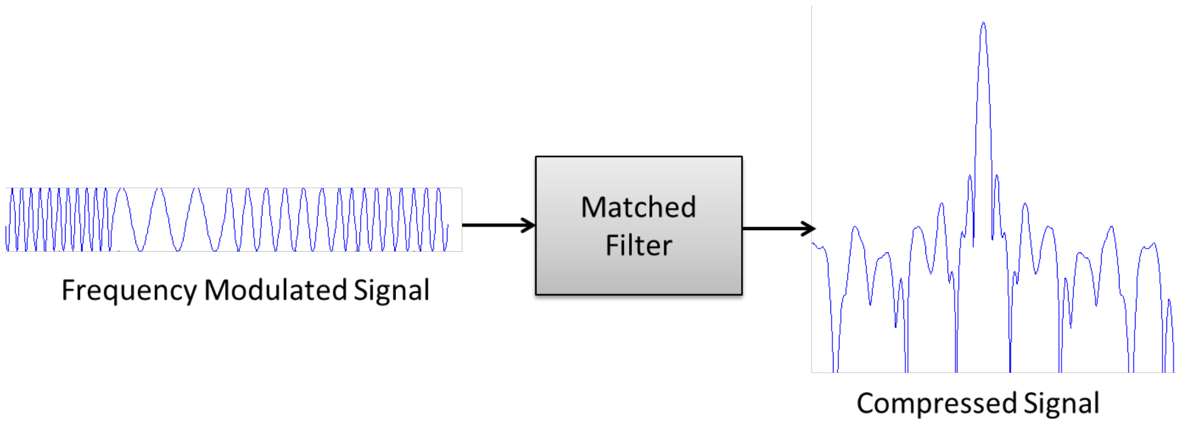

Figure 2. The Matched Filtering Process

Costas codes are named after John P. Costas, who published a report on their existence in 1965. Costas codes can be envisioned as points within a square grid checkerboard where each row or column contains only one point, and distances between each pair of dots are distinct. The unique relationships between the values within the Costas code result in a near ideal thumbtack auto-ambiguity function as shown in Figure 3 [8].

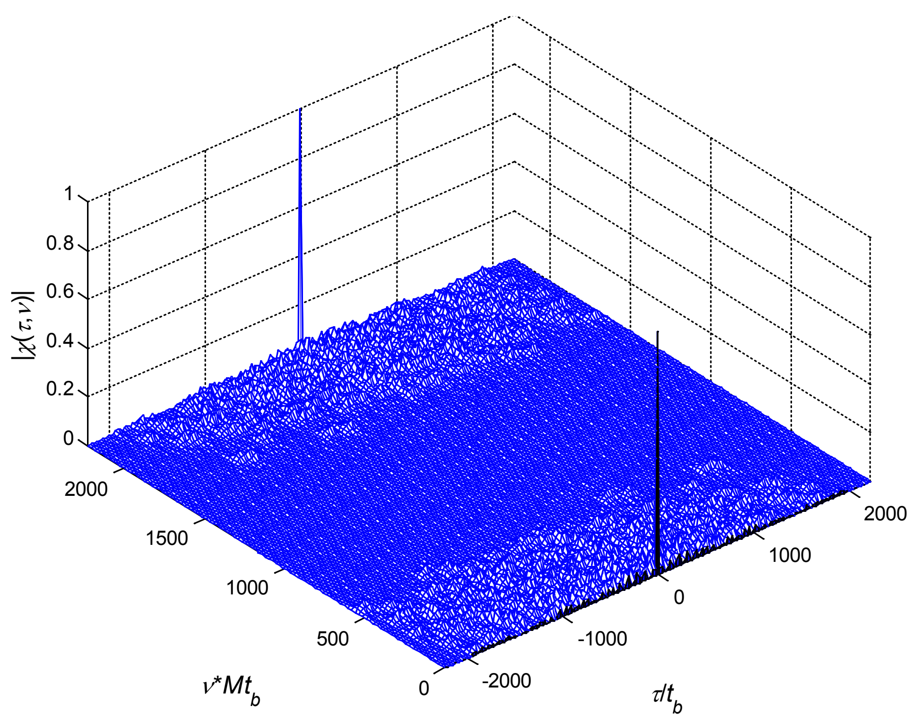

Figure 3. The Ambiguity Function of a Length-25 Costas Code

D. PREVIOUS WORKS

In this thesis, we build upon prior investigations of low probability of intercept (LPI) waveform applicability to SAR imaging. Giusti and Martorella [9] have used LPI Frequency-Modulated Continuous Wave (FMCW) waveforms in order to generate Inverse SAR (ISAR) images. In [10] and [11], Garren, Pace, and Romero investigated phase-shift keying (PSK) SAR techniques via the use of P3 and Frank codes. In [12] Lang extended the investigation of PSK techniques to include P1, P2 and P4 codes. The investigation of LPI waveforms for SAR imaging was extended to include frequency-hopping waveforms in [13], which forms the basis for this thesis. Costas-coded waveforms, which are another type of LPI waveform, are investigated in this thesis for applicability to form spotlight-mode SAR [1], [2], [14]–[16] images of a stationary scene.

E. RESEARCH OBJECTIVES AND APPROACH

The primary objective of this thesis is to determine the viability of using frequency diverse Costas-coded transmission waveforms in order to generate SAR images. A focus of the suitability of frequency-hopping waveforms for generation of SAR images is the impact of sidelobes. SAR images are degraded by either an excessive number of sidelobes or high sidelobe levels relative to the main lobe; therefore, the investigation of the sidelobe structure of Costas coded waveforms is a focus of this thesis. The expected benefit of this analysis is a demonstration of the overall viability of using LPI Costas waveforms in forming SAR imagery.

The overall approach is this analysis is to use simulated Costas waveforms in order to generate the expected radar return data based upon idealized point scattering centers placed in the scene. These simulated radar returns are ingested within an actual SAR image formation algorithm in order to determine the effectiveness of using Costas waveforms to generate useful SAR imagery. We look at the sidelobe effects, both in the two-dimensional (2D) imagery as well as one-dimensional (1D) slices in both the down-range and cross-range direction. It is necessary to confirm that the resulting sidelobes near main scattering centers are sufficiently low so as to avoid interfering with closely-spaced neighboring scattering centers. Costas waveforms of varying code length are used in the generation of

SAR images through MATLAB simulation. It is also important to confirm that this approach is viable for much longer Costas sequences, which will likely be required for a real imaging system. The resulting images are analyzed by extracting parameters to quantify the quality of the image.

F. THESIS OUTLINE

In Chapter II, the principles of SAR are presented to include the theory of spotlight mode SAR and the processing algorithms used to generate images. In Chapter III, the methodology of the SAR simulation and the setup of the simulation are presented. The simulation results are presented and analyzed in Chapter IV to show the correlation between the Costas sequence length and the autocorrelation side lobe levels. A summary of the thesis is presented in Chapter V along with recommendations for future work.

THIS PAGE INTENTIONALLY LEFT BLANK

II. TECHNICAL BACKGROUND

A. PRINCIPLES OF SYNTHETIC APERTURE RADAR

Side-looking radar can be used to generate images by flying an aircraft past the area to be imaged [1], [2]. As the aircraft proceeds along the flight path, the radar transmits pulses of RF energy which are reflected off the image area and returned to the radar. Each pulse of RF energy is transmitted at a different point along the flight path, and the antenna beam width is illuminating a different area on the ground. The two dimensions of a SAR image are the cross-range direction, which is the direction parallel to the flight path of the aircraft, and the range direction, which is perpendicular to the flight path of the aircraft.

Each pulse is received and processed using standard radar processing. This provides the data for the range direction [1]. A long pulse, when modulated, is used with pulse-compression techniques to improve range resolution while keeping transmit power requirements low. If the beam width is sufficiently small such that the cross-range resolution meets the image requirements, then this processing is all that is required [2]. This is the operation of a real-aperture system. As seen in Figure 4, a real-aperture system uses standard radar processing to generate range information and uses multiple collections along the flight path to generate the cross-range component of the two-dimensional image. A real aperture imaging system is limited in cross-range resolution by the beamwidth of the aperture. Each radar pulse must be transmitted from a location that is greater than the size of the beam on the ground

In the real-aperture system, the cross-range resolution is based on the horizontal angular beam width of the antenna and the range of the aircraft from the location being imaged as given by

$$W_{cr} = R\beta = R\left(\frac{\lambda}{D}\right), \qquad (1)$$

where R is the range between the aircraft and imaging area, β is the nominal angular width of an antenna in radians, the wavelength λ divided by the horizontal width of the antenna D [2].

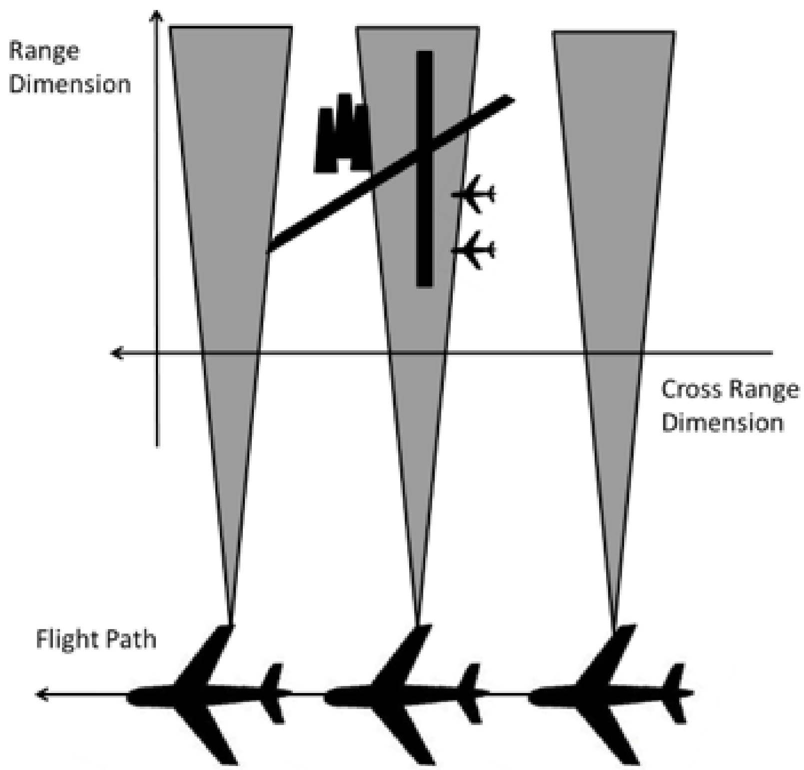

Figure 4. Image Formation Using the Real Aperture Imaging System

As an example, a system with a frequency of 3 GHz (0.1 m wavelength) and a 1.0-m antenna operating at a range of 50 km, from (1) has a cross-range resolution of

$$W_{cr} = R\beta = R\left(\frac{\lambda}{D}\right) = \left(50\times10^{3}\right)\left(\frac{0.1}{1}\right) = 5000 \text{ m} . \tag{2}$$

Clearly, a cross-range resolution of 5.0 km does not provide sufficient resolution to generate images useful in tactical military applications.

The methods for improving cross-range resolution of a real-aperture system are to reduce the range of the aircraft to the imaging location, reduce the wavelength, or increase the size of the antenna. Reducing the range is not feasible for satellite or most military applications. Wavelength is constrained by many other parameters such as propagation effects and manufacturing capabilities, and an antenna large enough to provide 1.0-m resolution requires an aircraft 5000-m long. The limits of the real-aperture system are obvious.

SAR employs digital processing techniques to synthesize a much larger aperture than the size of the real aperture. As the aircraft moves past the imaged area, each radar collection provides data at different locations. It is the distance along the flight path that makes the synthetic aperture. The size of the imaged area is the width of the ground beam pattern since this is the distance that a point is within the beam along all points of the flight path. This means that the SAR system operates better with a smaller antenna as opposed to the larger antenna requirement of a real-aperture system. This leads to the smaller the antenna on the SAR system, the larger the imaged area, and the finer the cross-range resolution [17]. Using this method a synthetic aperture of several kilometers can be obtained, resulting in much finer cross-range resolution.

There are two major modes used in SAR: strip-map SAR and spotlight SAR as illustrated in Figure 5. Both modes use side-looking radars to image an area. In strip-map SAR, the antenna-pointing angle is fixed, and the beam of the radar passes over the imaged area as the aircraft flies over. In spot-light SAR, the antenna is steered to maintain the beam over the imaged area. The spotlight mode SAR is preferred when the area to be imaged is a small patch [1]. Under this condition, the spotlight mode SAR requires fewer pulses to image the area and allows for a larger antenna, which can provide more gain to make the overall system design easier. In this thesis, we focus on spotlight mode SAR, which is now described in more detail.

SAR systems must transmit consecutive waveforms at a spatial interval corresponding to one-half of the antenna beam-width to prevent aliasing due to under sampling [1], [2]. An example of the spotlight-mode geometry is shown in Figure 6. In strip-map SAR, a large number of pulses are required to image a small area. In Figure 6, the aircraft is traveling at 5 m/s, operating at a range of 70 km from the imaged area, travels a distance of 3.18 km, and images an area 1.0 km square. The system operates at a frequency of 10 GHz (0.03 m wavelength), and a 0.33 m resolution is desired. Geometry can be used to calculate the angular beam-width of 0.82 degrees, resulting in an antenna width of 2.1 m. To prevent undersampling, the radar must transmit consecutive waveforms at a spatial interval of one-half of the antenna beam-width, which corresponds to a distance along the synthetic aperture of 1.05 m. Taking the aircraft velocity into account, we see that the pulse-repetition frequency (PRF) must be at least 4.76 kHz.

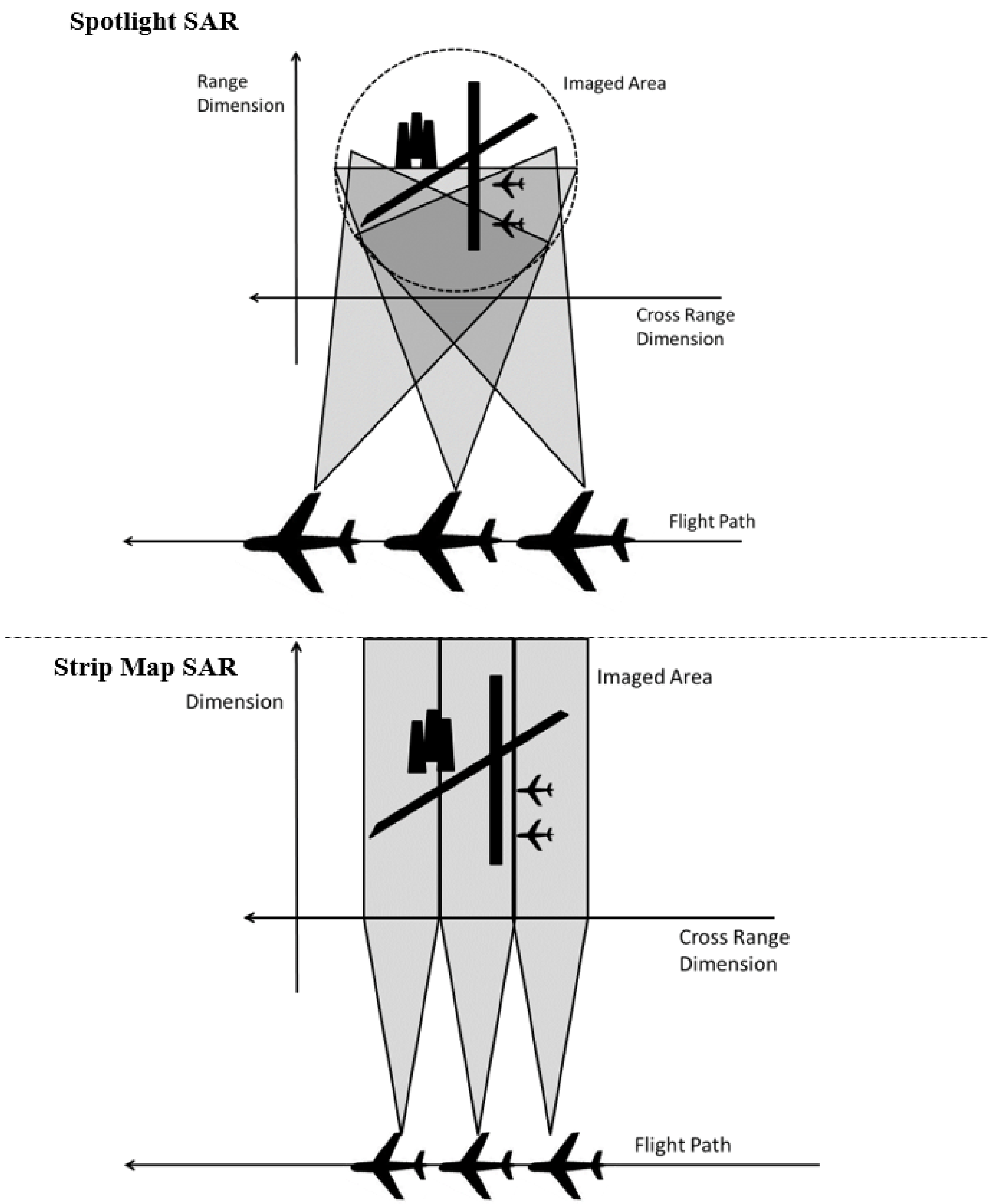

Figure 5. Two Primary Modes of SAR Are Spotlight SAR (above) and Strip Map SAR (below). Adapted from [2].

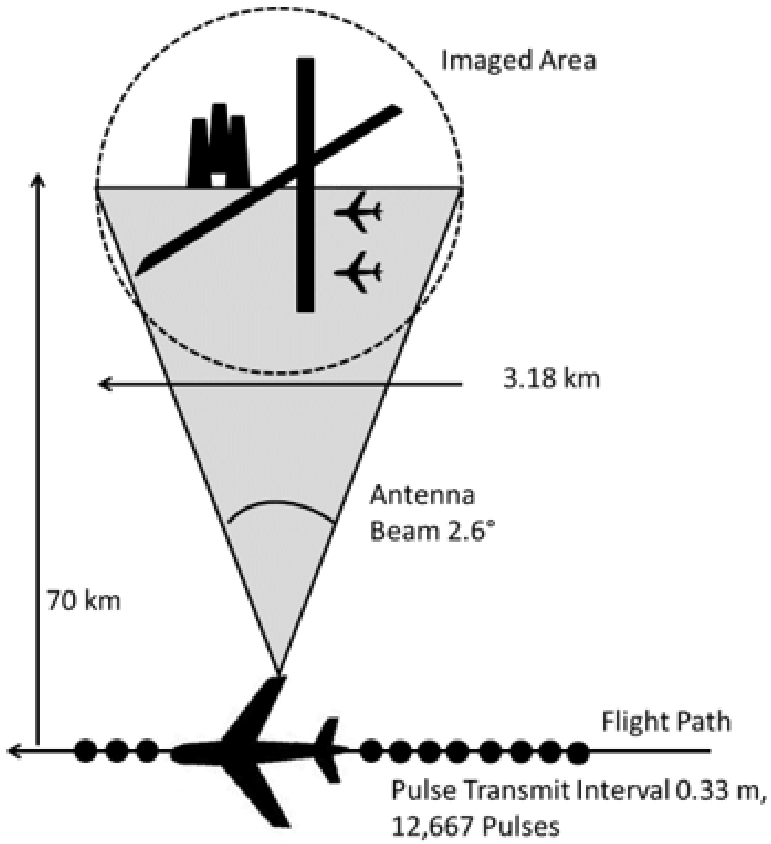

Figure 6. Pulse Collection in Strip-Map SAR. Adapted from [2].

B. SPOTLIGHT-MODE DATA COLLECTION

The collection of phase history data occurs in three-dimensional space, and the data must be translated into a two-dimensional image. In this section, we discuss the theory and process for transforming data collected in two-dimensional space into a two-dimensional image.

Phase data collected by the moving aircraft is represented on a slant plane. The slant plane dimensions are X' and Y'. The spatial coordinate Y' represents the slant-range spatial frequencies, and X' is orthogonal to Y' and lying in the plane. The angle ψ is the angle of the imaged area to the aircraft with respect to the ground. The angle θ is the squint angle and is measured from the imaging area to the aircraft with respect to the direction of travel. To form a ground plane image, these slant dimensions must be projected onto the ground plane. Several key relationships in the slant-plane are summarized in the following equations [2].

The range resolution is

$$\rho_{y'} = \left(\frac{2\pi}{\Delta Y'}\right) = \left(\frac{c}{2B_c}\right), \tag{3}$$

where c is the speed-of-light and B_c is the bandwidth of the signal. The range resolution can be no better than $\lambda / 4$ since the radar can never have a bandwidth that exceeds twice the center frequency. The cross-range resolution is

$$\rho_{x'} = \left(\frac{2\pi}{\Delta X'}\right) = \left(\frac{\lambda}{2\Delta\theta}\right). \tag{4}$$

The minimum sampling interval in the X' dimension required to build an image of diameter $2L$ without aliasing is given by

$$\delta X' = \left(\frac{2\pi}{2L}\right), \tag{5}$$

which results in the corresponding angular sampling interval of

$$\delta\theta = \left(\frac{\delta X'}{2\pi / \lambda}\right) = \frac{\lambda}{2(2L)}. \tag{6}$$

The along-track sampling interval in meters can be calculated as

$$\delta A = R\delta\theta = \frac{\lambda R}{2(2L)} = \frac{D}{2}, \tag{7}$$

where D is the width of the antenna that illuminates a ground region of $2L$ diameter. When the slant-plane is projected onto the ground plane, the range resolution becomes

$$\rho_y = \frac{2\pi}{\Delta Y} = \frac{c}{2B_c \cos\psi}, \tag{8}$$

where ψ is the angle of the imaged area to the aircraft with respect to the ground. The cross-range resolution then becomes

$$\rho_x = \frac{2\pi}{\Delta X} = \frac{\lambda}{2\Delta\theta}. \tag{9}$$

The cross-range resolution does not change between the slant-plane and ground plane. The range resolution is scaled by a factor of $\cos\psi$ when projected onto the ground plane.

The maximum dimensions of an area that can be imaged can be determined [1]. For the cross-range dimension, the maximum length of the image is a function of the slow-time sampling (the radar PRF given as N_x), the change in angle per pulse repetition interval (PRI), and the wavelength of the signal:

$$D_x = \frac{\lambda N_x}{2\Delta\theta}. \tag{10}$$

For the range direction, the maximum length of the image is a function of sampling in the fast-time, given as N_y, and the bandwidth of the waveform:

$$D_y = \frac{cN_y}{2B}. \tag{11}$$

C. SQUINT ANGLE

The angle from the imaging area to the aircraft with respect to the direction of travel is called the squint angle. The topic of squint angle is briefly discussed here because it does have an impact on the resulting image, but the simulations executed for this thesis are all centered on a broadside collection.

When the center of the imaged area is perpendicular to the synthetic aperture, the geometry is termed broadside. If the collecting platform position is prior to the broadside geometry, then the collection is a forward squint. After the platform has passed, the broadside geometry the collections are back squint, as shown in Figure 7.

D. THE RANGE DOPPLER ALGORITHM

The processing of phase-history data into an image is done with the Range Doppler Algorithm (RDA). The RDA uses Fourier transforms, typically via Fast Fourier Transform (FFT), in the range and cross-range dimensions to form an image from the phase history data [18]. A diagram of the RDA is shown in Figure 8.

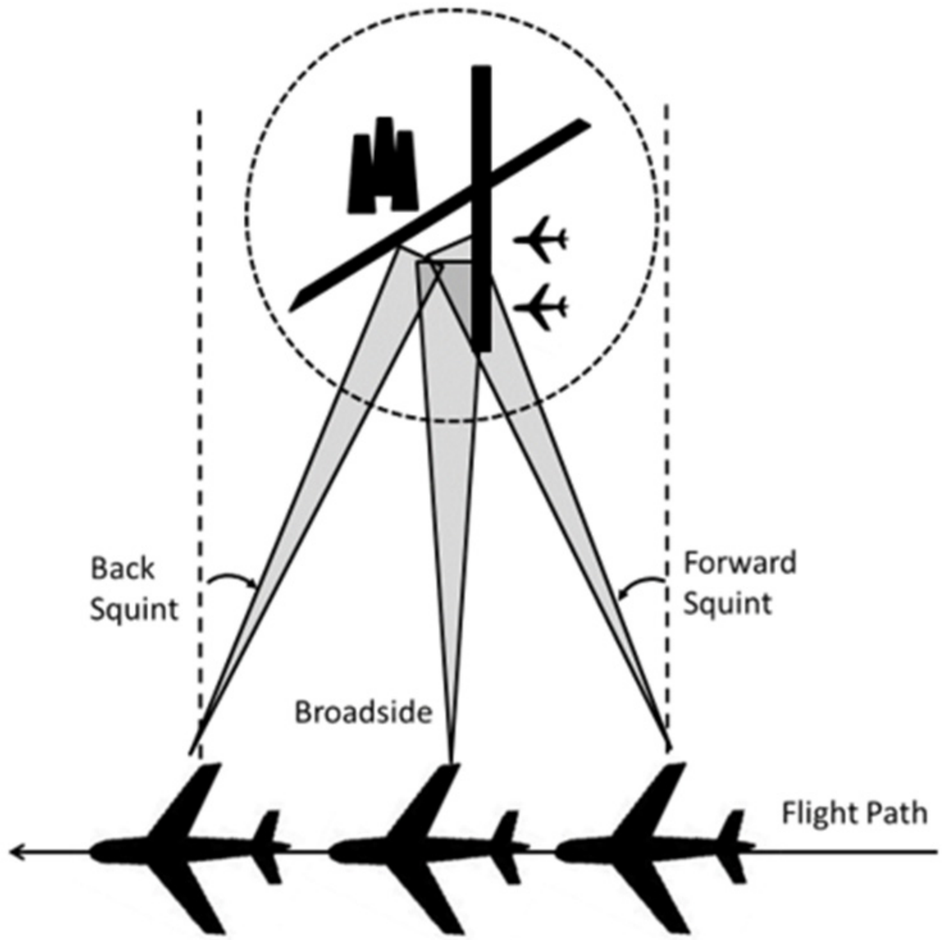

Figure 7. Forward and Back Squint in Strip-Map SAR. Adapted from [2].

The first process in the RDA is the processing of the phase data in the range dimension. Pulse compression is performed through matched filtering via convolution. The received signal is processed through an FFT in the range dimension to convert to the time domain. The signal in the range dimension is convolved with the conjugate, time-reversed version of the transmitted signal. The output of the convolution process is the pulse compressed signal in the range dimension.

The resulting signal is processed through an inverse Fourier Transform via the Inverse Fast Fourier Transform (IFFT) to convert the signal back into the frequency domain in the range dimension. It is possible to take this output and perform a two-dimensional

FFT to generate an interim image, but without the polar-to-rectilinear processing, the image is typically distorted [2], [18].

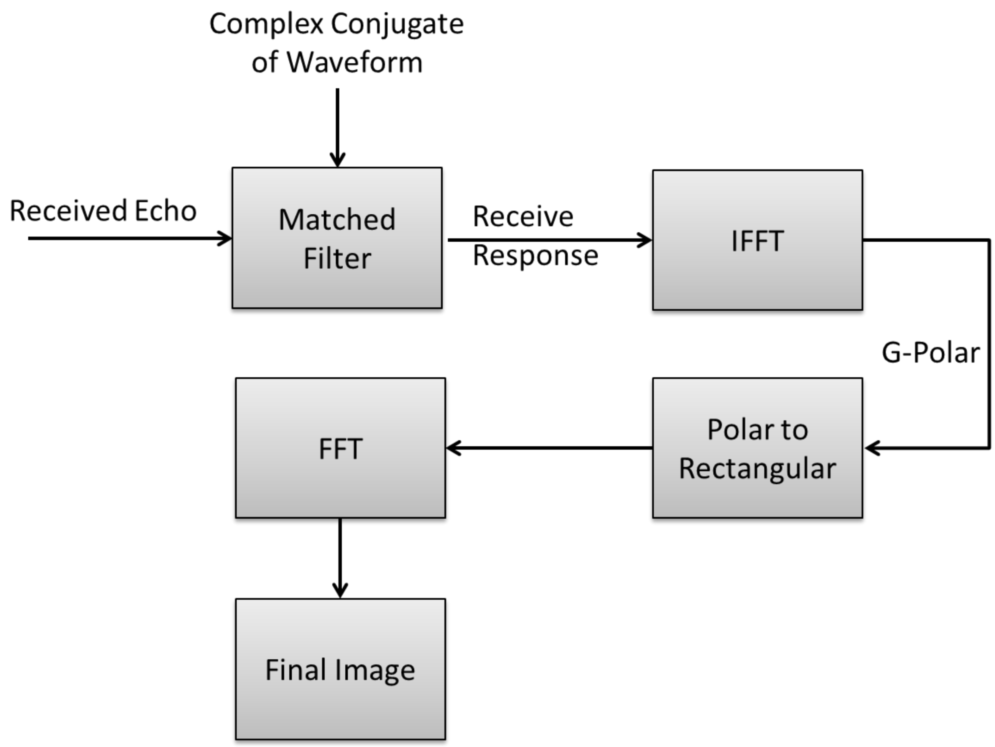

Figure 8. Block Diagram of the Range Doppler Algorithm

The next step is the polar-to-rectilinear transformation, after which a windowing function can be applied. Finally, a two-dimensional FFT is performed to convert both range and cross-range to the time domain, which forms the final image.

E. POLAR-TO-RECTANGULAR CONVERSION

The phase history data collected in the spotlight SAR mode is polar formatted. The key processing that occurs during the RDA is the FFT; however, the FFT requires uniformly spaced data on a rectangular grid; therefore, to utilize the processing efficiency of the FFT, the phase history data must be converted from its inherent polar format to a rectangular format [2].

The process for converting from polar to rectangular is a two-step process. The first step is range interpolation as shown in Figure 9. The samples on the radial lines are interpolated onto a trapezoidal grid. After this interpolation step, the samples remain on the radial lines (cross-range is still polar). The samples are now interpolated onto the rectangular grid for the range dimension and referred to as keystone samples.

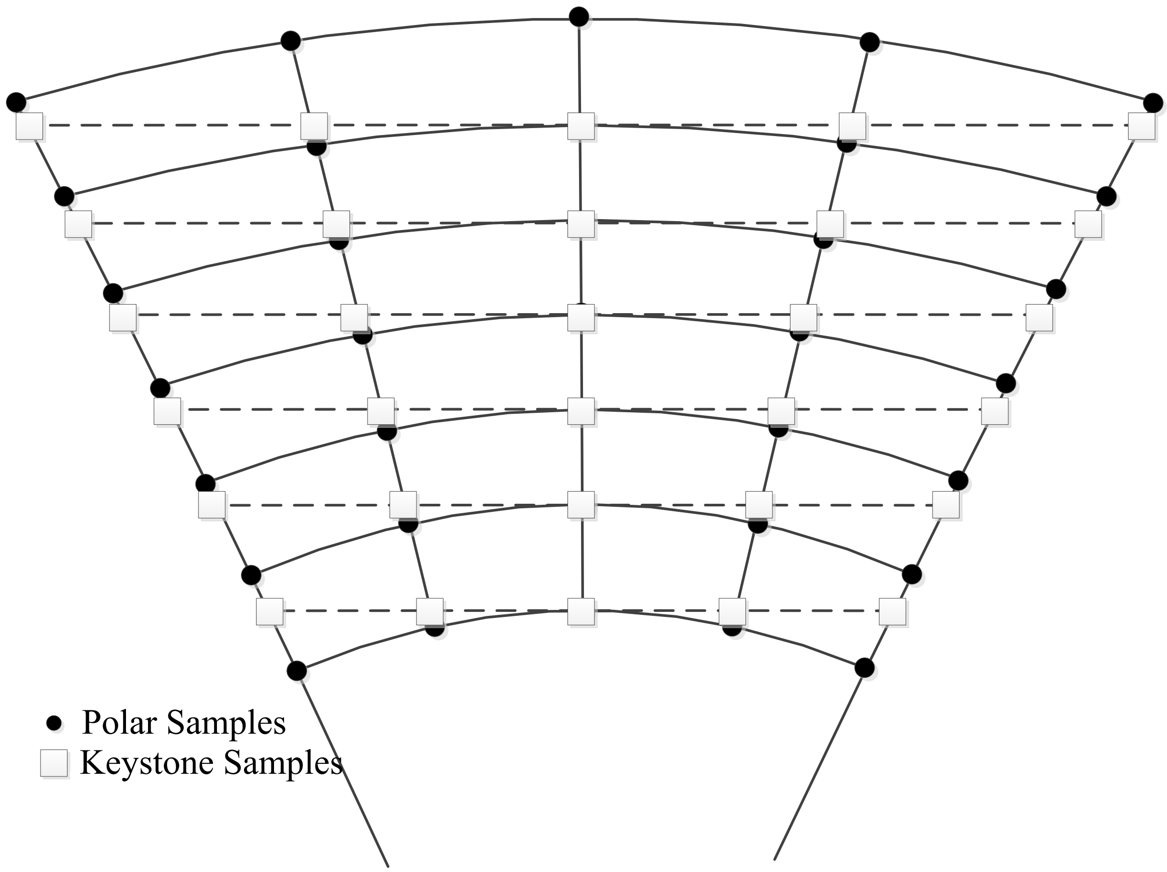

Figure 9. Conversion of Polar Samples to Keystone Samples. Adapted from [2].

The second step is the cross-range interpolation as shown in Figure 10. The keystone sampled data are interpolated on the final rectangular grid. The process of breaking the polar-to-rectangular conversion into two steps simplifies the process into two nearly identical interpolation steps.

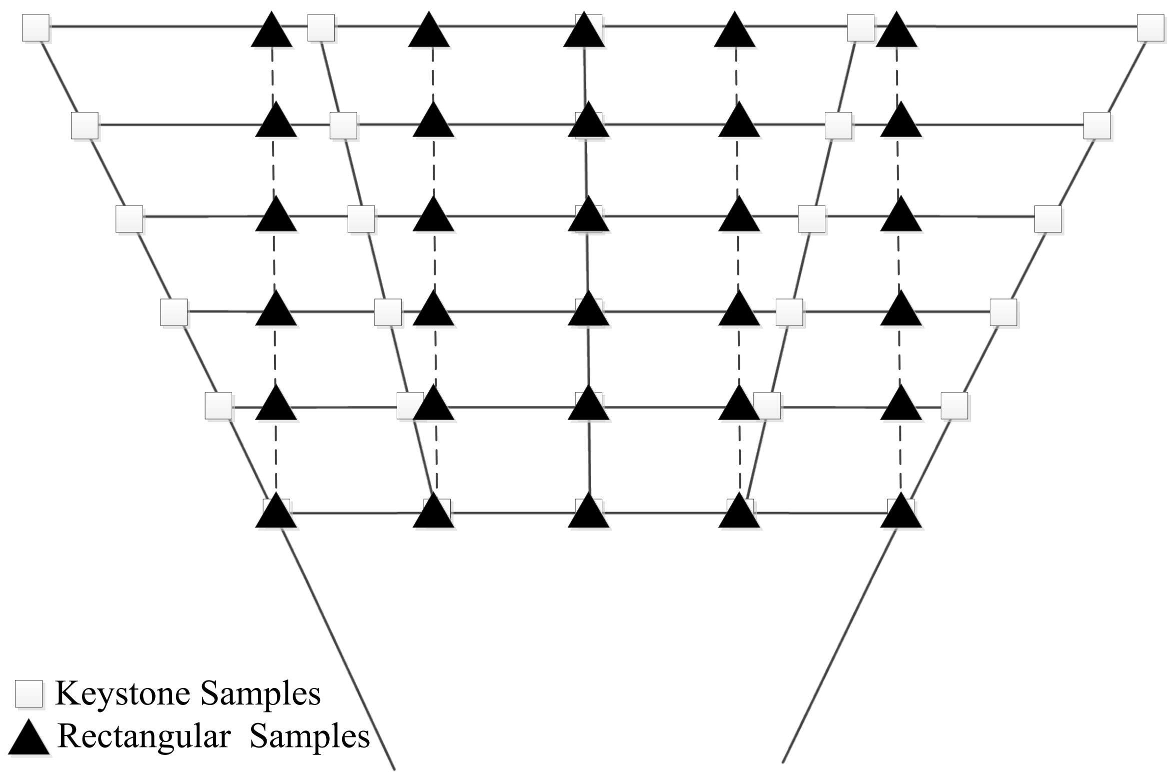

Figure 10. Sampling of Keystone Samples onto the Final Rectangular Grid. Adapted from [2].

F. PRINCIPLES OF COSTAS-CODED WAVEFORMS

Parts of this section were previously published in *Proc. of the IEEE Radar Conference, 2017* [13].[1]

Costas coding is a method for generating waveforms that use frequency-shift keying (FSK) or frequency hopping. Costas codes are a highly optimized set of codes that, when used with matched filtering, produces high compression values with low sidelobes [8], [19]. The Costas coded waveforms examined in this thesis are Costas-coded pulses

[1] Reprinted, with permission, from Z. Wagner, D. Garren, and P. Pace, "SAR imagery via frequency shift keying Costas coding," in *Proc. of the IEEE Radar Conference*, Seattle, WA 2017. This publication is a work of the U.S. government as defined in Title 17, United States Code, Section 101. Copyright protection is not available for this work in the United States. IEEE will claim and protect its copyright in international jurisdictions where permission from IEEE must be obtained for all other uses, in any current or future media, including reprinting/republishing this material for advertising or promotional purposes, creating new collective works, for resale or redistribution to servers or lists, or reuse of any copyrighted component of this work in other works.

transmitted at a fixed PRI. Each pulse of length τ' is divided into N subpulses of equal duration τ_1. Each subpulse is at a different frequency. The time-bandwidth product for a Costas code is

$$\Delta f \tau' = N^2 \ . \tag{12}$$

The pulse compression ratio for a Costas code, which is the ratio of the uncompressed pulse width to the compressed pulse width, is given by

$$PCR = N \ . \tag{13}$$

An example Costas-coded pulse with a Costas sequence with sequence length six is shown in Figure 11.

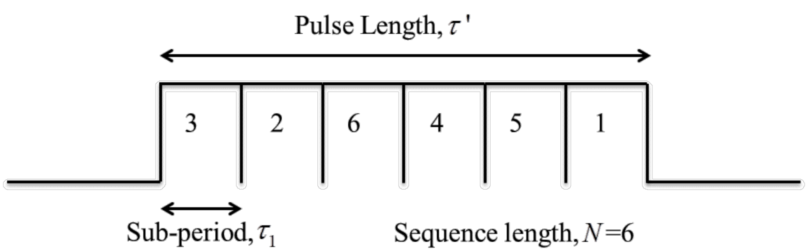

Figure 11. A Six-Sequence Costas-Coded Pulse

The sequence of the frequencies is set by the Costas sequence. The key feature of the Costas code is that each frequency is used only once during the code. This can be visualized as an N by N matrix. The columns are indexed as $i = 0,1,2,...,N-1$, and the rows are indexed as $j = 0,1,2,...,N-1$. Each row represents a subpulse, and each column represents a frequency. A dot in a particular box indicates the frequency of that particular subpulse. The frequency matrix for a six-level Costas code is shown in Figure 12. The Costas sequence represents an index that is a multiplier to a base frequency to obtain the individual sequence frequencies.

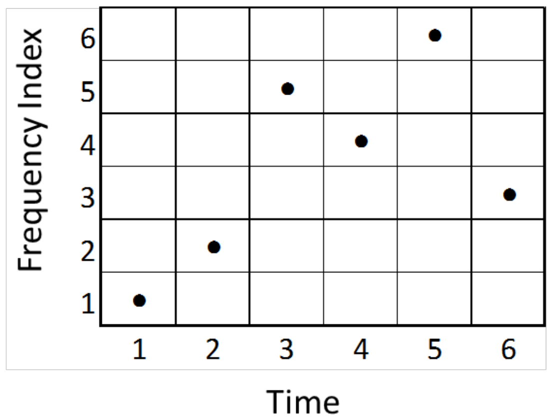

Figure 12. A Binary Time-Frequency Matrix for Costas Sequence {1,2,5,4,6,3}

Another key feature of the Costas code is that time and frequency shifted copies of the matrix produce only one coincidence at most outside of the origin. This is because the matrix has only one entry per row and column and the distances between each pair of dots are distinct [8], [19]. This results in the low sidelobe performance ideal for radar applications. This concept is shown in Figure 13. As the frequency matrix with the white squares is shifted in time and frequency, there is only one square containing both a circle and a square within this matrix. This property of Costas codes results in the near ideal thumbtack auto-ambiguity function [8].

A key condition of the Costas code is the orthogonality requirement, meaning that there is no overlap between the sub-channels. Orthogonality is satisfied by

$$\tau_1 N = 1. \tag{14}$$

For a given subpulse duration τ_1, the frequency-hopping separation is the inverse of τ_1. For the example waveform given above, a subpulse duration of 10.0 ns requires a frequency-hopping separation of 100 MHz.

There are multiple methods for determining a Costas sequence, with the Welch construction and the Golumb construction being two of the more popular methods. A database of known Costas arrays by James K. Beard is available and has been extensively leveraged for the MATLAB simulations in this thesis [20].

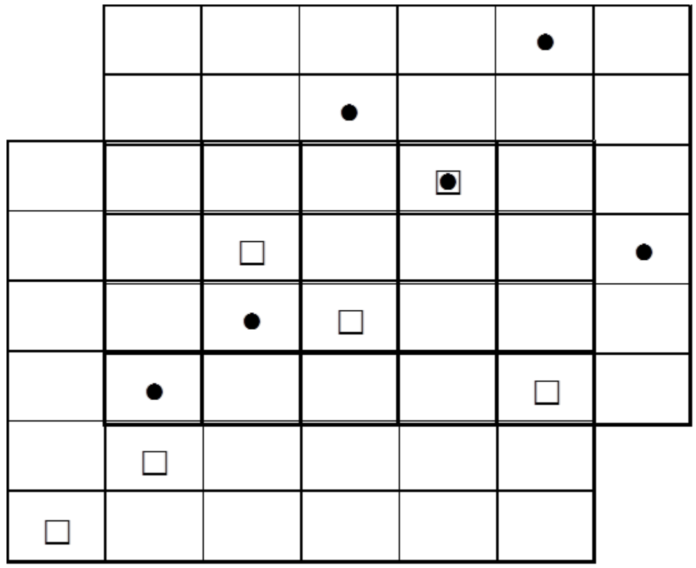

Figure 13. Time and Frequency Coincidence of a Six-Sequence Costas Code

In this chapter, the principles of SAR were introduced with a focus on spotlight mode data collection, the type of SAR investigated in this thesis. In this chapter, the processing algorithms required to generate images from SAR were also discussed. These processing algorithms form the foundation of the SAR simulations which are discussed in the next chapter.

III. SIMULATION METHODOLOGY

For this thesis, several Costas waveforms are used to characterize their performance with SAR. To isolate the impact of a particular parameter on the formation of a SAR image, only a single variable is modified at a time. This design of experiments methodology provides excellent characterization of the waveforms; however, it increases the amount of time required to perform the characterization and, therefore, limits the degrees-of-freedom examined. The parameters of the Costas waveforms that were characterized were the Costas code sequence length and the subpulse period, which directly impact the waveform bandwidth. A complete table of the sequences used in this thesis is given in Appendix A. The waveform parameters used in this thesis are given in Table 1 along with some derived parameters.

Table 1. List of Waveforms and Parameters

Waveform Number	Costas Sequence Length	Costas Sequence Number	Subpulse Bandwidth (MHz)	Total Waveform Bandwidth (MHz)	Total PW (μs)	PRI (ms)	Transmit Duty Cycle (%)
1	15	1	10	150	1.5	43.5215	0.0034466
2	15	2	10	150	1.5	43.5215	0.0034466
3	15	3	10	150	1.5	43.5215	0.0034466
4	15	4	10	150	1.5	43.5215	0.0034466
5	15	5	10	150	1.5	43.5215	0.0034466
6	100	6	1.5	150	66.6	43.4322	0.1535
7	100	7	1.5	150	66.6	43.4322	0.1535
8	100	8	1.5	150	66.6	43.4322	0.1535
9	100	9	1.5	150	66.6	43.4322	0.1535
10	100	10	1.5	150	66.6	43.4322	0.1535
11	150	11	1	150	150	43.327	0.34541
12	150	12	1	150	150	43.327	0.34541
13	150	13	1	150	150	43.327	0.34541
14	150	14	1	150	150	43.327	0.34541
15	150	15	1	150	150	43.327	0.34541

A. SPOTLIGHT SAR SIMULATION SETUP

A MATLAB simulation is used for characterizing the performances of Costas coded waveforms on SAR image formations. In the MATLAB simulation, the number of variables is constrained to keep the focus on the impact of the varying Costas waveforms. A list of parameters in the SAR simulation is given in Table 2.

Table 2. SAR Simluation Parameters

Parameter	Symbol	Value
Radar Platform Velocity	V_p	200 m/s
Radar Platform Height	H_p	6096 m
Depression Angle	ψ	13°
Ground Range	θ_{si}	30.0 km
Radar Center Frequency	f_0	2.0 GHz
Collection Time	T	1.0 s
Platform Direction	D	1 = Right to left
Number of Frequency Samples	*NumSR*	250
Number of Waveforms	*NumSCR*	250

The spotlight SAR MATLAB simulation is configured as two components. The first component is the code that generates the images from several inputs. The code segments used in the simulation are given in Table 3 along with a brief description.

Table 3. Primary Modules Used in the Simulation of SAR Images

Function	Overview
Run_SAR_Extract_One_Simulated_Chip_V2.m	Top-level routine to generate SAR images. This routine is a modified version of the code generated by Professor Garren. Executes the RDA on the specified scattering centers and generates images.
Simulator_Generator_Scattering_Trajectories1.m	Specifies the scattering centers to be used in the scene. Scene index is passed in from the top-level routine and returns an array of scattering center trajectories.
Simulator_Get_Radar_Sensor_Parameters.m	Specifies radar parameters including range, elevation, squint angle, frequency, imaging duration, and speed. It reads in the Costas sequence, as passed-in from the top-level routine, and sets-up other waveform parameters.
Plot_Image_with_Spatial_Axis_V2.m	Generates SAR image from the output of the RDA. Applies FFT padding, if specified, to improve SAR image quality. A Hanning window can also be applied to the data if specified.
Simulator_Initialize_Params.m	Top level simulator parameters including Debug, sets PI and J, and speed of light.
Extract_Image_Chip_V2	Called from the top-level routine. Prepares data for image generation. Call Plot_Image_with_Spatial_Axis_V2 for the full image and a "zoomed" image.
Intialize_Global_Params.m	Specifies global parameters to be used in the simulation.
CostasFunction.m	Called from the radar sensor parameters function. This is the Costas IQ generator from the LPI Toolbox rewritten as a function. The function generates a Costas waveform based on the parameters passed-in.

The core spotlight SAR algorithm is nested in several looping structures. The looping structures provide a mechanism to automate generation and data collection of the SAR images. There are three primary loops. The first, most outer, loop is the scattering center position loop. This loop generates scattering trajectories based on the loop index.

This allows for different scattering scenes to be simulated. In this simulation, there are two scattering scenes as given in Table 4.

Table 4. Definition of Scattering Scenes

Scattering center Scene	**Position (Range, Cross Range) in Meters**
1	40, 35
2	0.14, 0.0; 40.0, 35.0; −28.2, −17.8; 12.7, −21.5; −33.1, 8.2

The second loop is the Costas code sequence length. The input to this loop is a vector of Costas code lengths. As an example, to generate data for Costas codes of length 3, 9, 15, 18 and 25 the vector is

TestSequenceLengths = [3,9,15,18,25].

The third loop is the number of waveforms to simulate at each Costas code length. Several different waveforms at each Costas code length can be simulated by specifying a value greater than 1 in order to determine if the actual code has an impact on the formation of an image. The simulation uses the loop index as a lookup into a table of sequences. The lookup into the Costas code sequence table is determined by dividing the total number of waveforms to be simulated by the total number of sequences in the table for that particular Costas code length and multiplying by the index. This method selects sequences at equal intervals in the table and prevents the codes used in the simulation from being very similar.

For example, there are 40 Costas code sequences of length five. The first pass through the loop, the index is one and the first code is always selected. The second pass through the loop, the index is two and the twentieth code is selected. On the last pass through the loop, the last code is always used. If the number of waveforms to be tested exceeds the number of waveforms available at that particular Costas code length, the simulation exits out of the loop when all Costas codes at the selected length have been simulated.

The fourth, and most inner, loop is an additional test parameter to be simulated. This test parameter is specified in a header, and the simulation reacts accordingly. Testing with the selected test parameters requires additional updates to the MATLAB code. The indexes of the subpulse period loop are a vector of subpulse periods to be simulated.

The second component to the MATLAB simulation is the data reduction code. This code loads a specified Sequence structure, performs calculations of Peak Side Lobe Ratio (PSLR) and Integrated Side Lobe Ratio (ISLR), and generates range and cross-range profile plots.

B. RANGE PROFILE PLOTS

A range profile is a slice of a single range from the 2D image produced at the output of the SAR image algorithm. An example of a range profile for a length-15 Costas sequence is given in Figure 14. The x-axis is range in meters. The center of image is at 0.0 m. In this example, the image is 250 m in range with the center of the image at 0.0 m, the portion of the image closest to the sensor at -125 m, and the portion of the image farthest in range at +125 m.

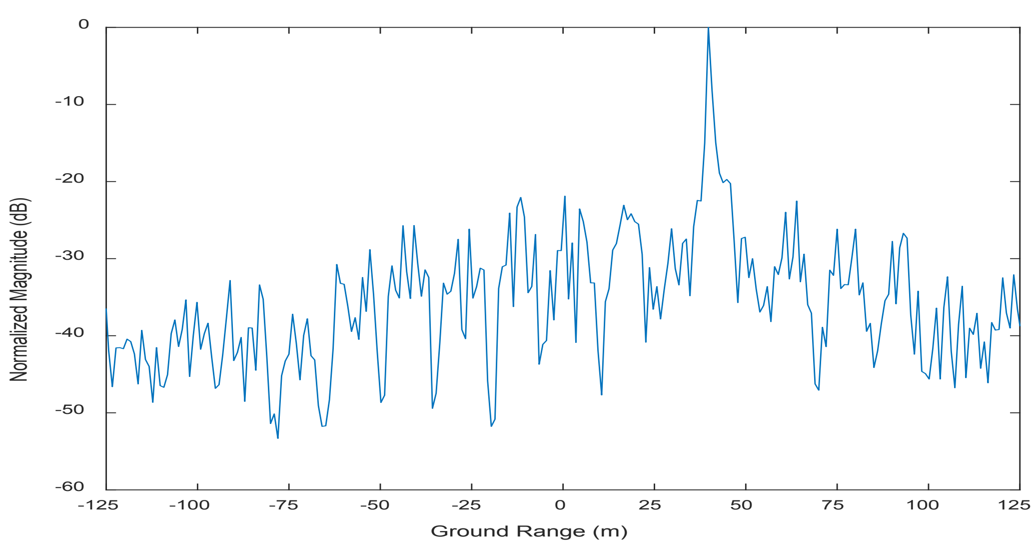

Figure 14. Example of a Ground Range Profile

C. CROSS-RANGE PROFILE PLOTS

The cross-range profile plots are generated identically to range profile plots. The cross-range profile typically does not exhibit the variation in sidelobe structure that is shown in the range profile. An example of a cross-range profile plot for a length-15 Costas sequence is given in Figure 15.

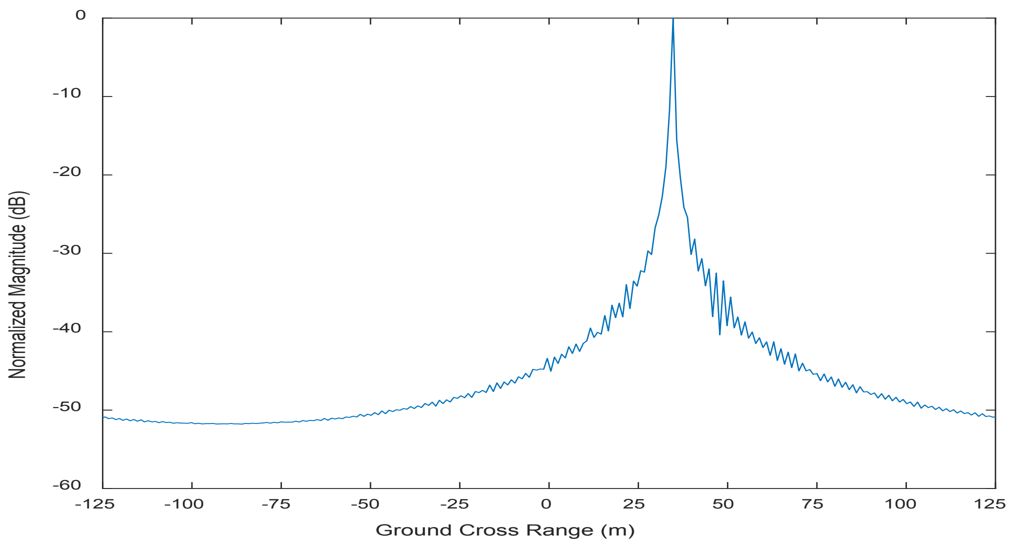

Figure 15. Example of a Ground Cross-Range Profile

In this chapter, the setup of the SAR simulator and the key parameters within the simulations were presented. In the next chapter, the images from the SAR simulator for three different lengths of Costas sequences are presented and analyzed.

IV. SIMULATION RESULTS

The simulation results are presented as a detailed analysis of a single scattering center position as a function of number of subpulses. Three waveforms of increasing subpulse length are analyzed using the MOPs outlined in the previous section, and a qualitative analysis is performed on the resulting image. The impact of multiple scattering centering centers in an image scene is then examined using the same three waveforms to analyze the effect of subpulse length on image quality.

A. DETAILED SINGLE SCATTERING CENTER ANALYSIS

1. Length-15 Costas Code

The first single scattering center image was generated using the parameters given in row one of Table 1. The resultant image in Figure 16 from the length-15 Costas code corresponds to the case of the Table 1 point scattering center at the expected location. The 100 dB of dynamic range within the image allows the sidelobe structure in both range and cross range to be clearly visible. The image slices through the scattering center in range and cross-range capture the sidelobe structures across the image.

From the range profile plot in Figure 17, the position of the peak in range is as expected. The peak sidelobes are not well defined, as they are very near the main lobe and are not as pronounced as the other sidelobes further from the main lobe; however, the application of the near-in sidelobes yields PSL values of -28 dB on the left and -24 dB on the right. The sidelobe structure of the range profile is as expected. For the length-15 Costas code waveform with a 150-MHz bandwidth, each subpulse has a 10-MHz bandwidth. A 10-MHz bandwidth results in a 15-m resolution. The length of the image is 250 meters, and when divided by the 15-m resolution, we expect to see approximately 16 lobes in the range profile, seen in Figure 17.

The cross-range location is as expected within the cross-range plot of the length-15 Costas code in Figure 18. There is minimal sidelobe structure in the cross-range direction. This is not an artifact of the FSK waveform as other types of waveforms show similar behavior.

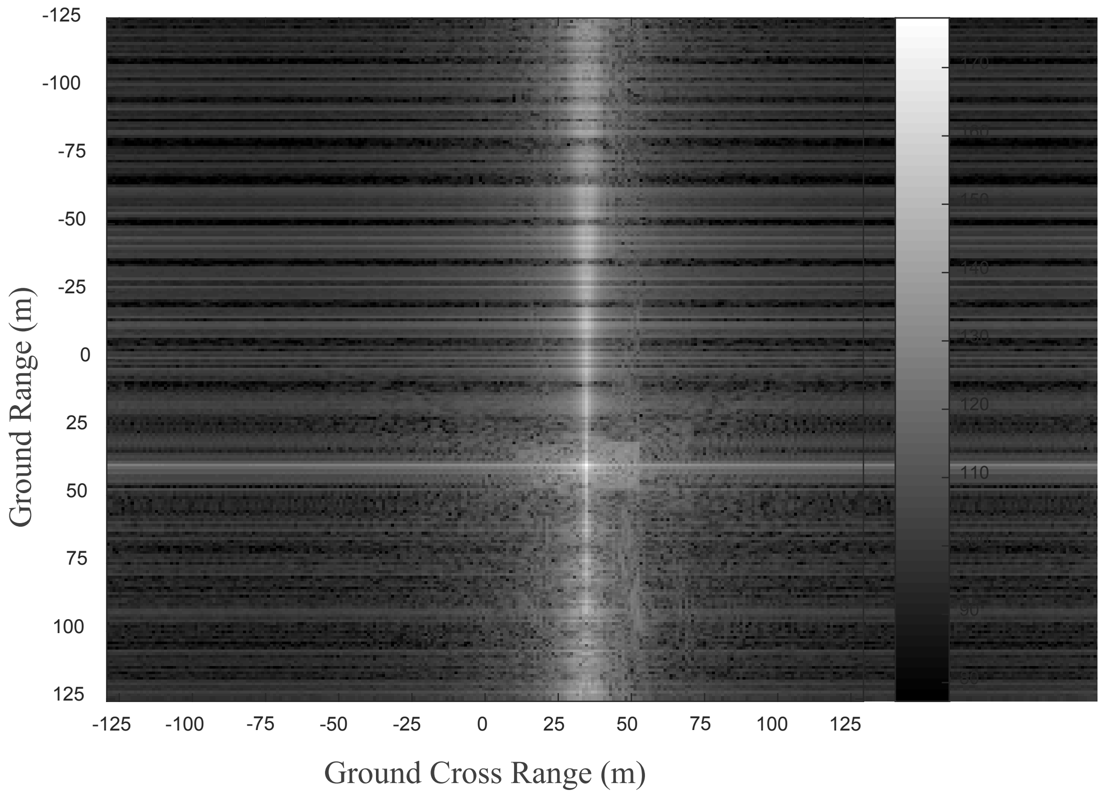

Figure 16. Length-15 Costas Code SAR Image of a Single Scattering Center Using the Parameters Defined in Table 1, Row One

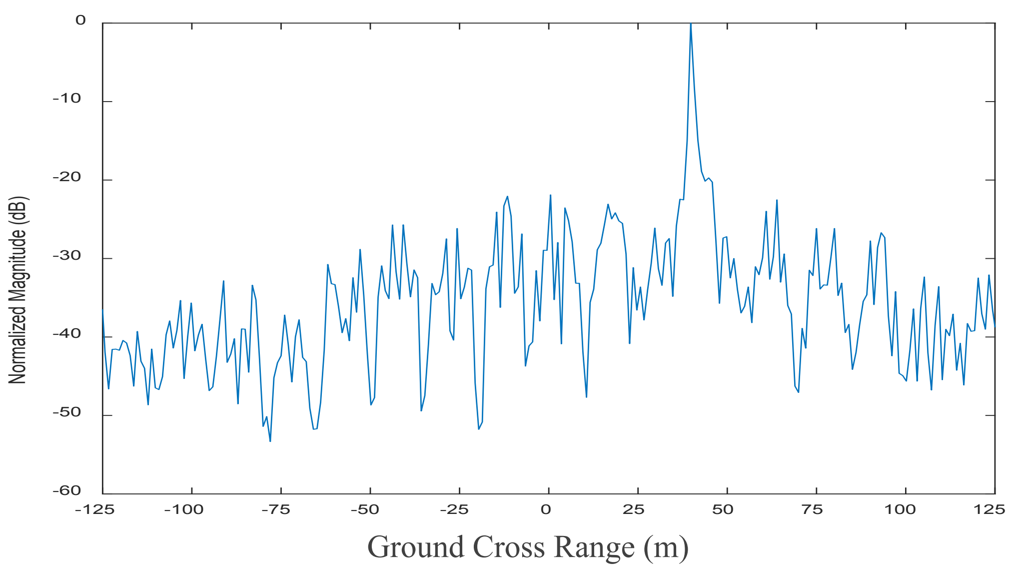

Figure 17. Length-15 Costas Code SAR Image Range Profile Slice of a Single Scattering Center Using the Parameters Defined in Table 1, Row One

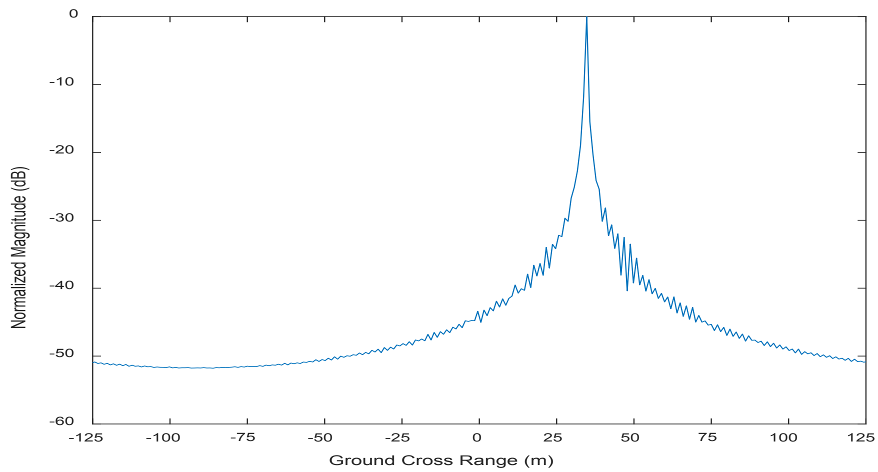

Figure 18. Length-15 Costas Code SAR Image Cross-Range Profile Slice of a Single Scattering Center Using the Parameters Defined in Table 1, Row One

To examine the dependence of image performance on unique Costas codes, five unique Costas codes were run through the SAR image generator. The resultant images are shown in Figure 20. In all of the images, the single scattering center is clearly visible, and there are no major differences between the images. Closer inspection of the images reveals slight differences in the background generated by variations in the range sidelobe structure, as seen by the overlay of all five ground range profiles in Figure 19.

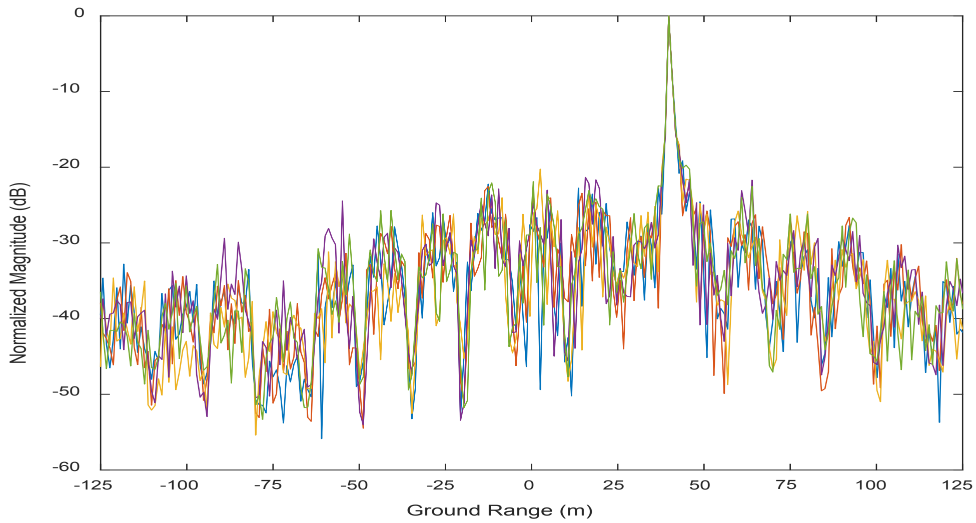

Figure 19. Overlay of Five Unique Length-15 Costas Code SAR Image Range Profile Slices of a Single Scattering Center Using the Parameters Defined in Table 1, Rows 1–5

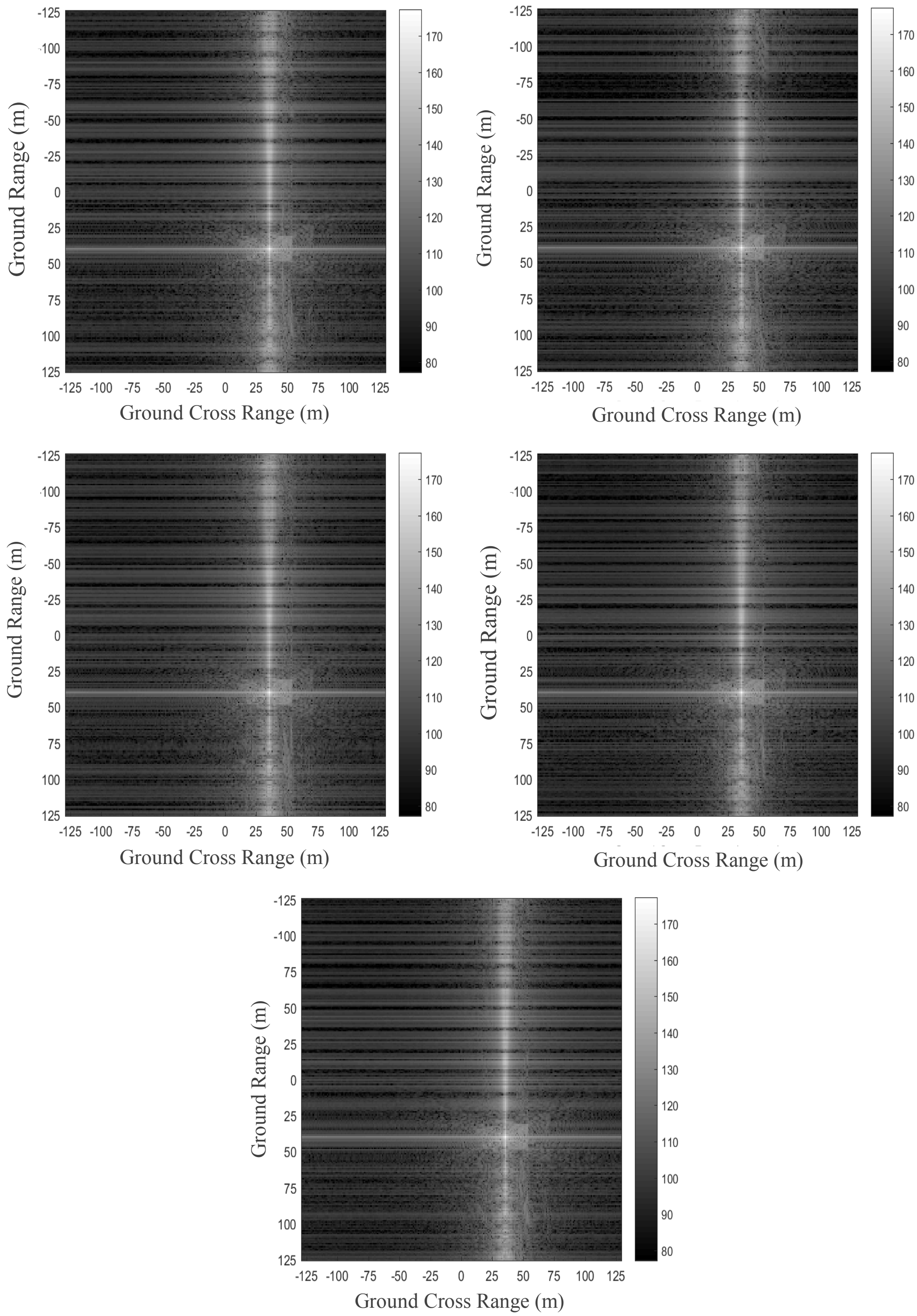

Figure 20. SAR Images of a Single Scattering Center Resulting from Five Unique Length-15 Costas Codes Using the Parameters Defined in Table 1, Rows 1–5

2. Length-100 Costas Code

The length-100 Costas code from row 6 in Table 1 results in the single scattering center image shown in Figure 21. The scattering center is located in the expected position within the 1.0 m resolution tolerance.

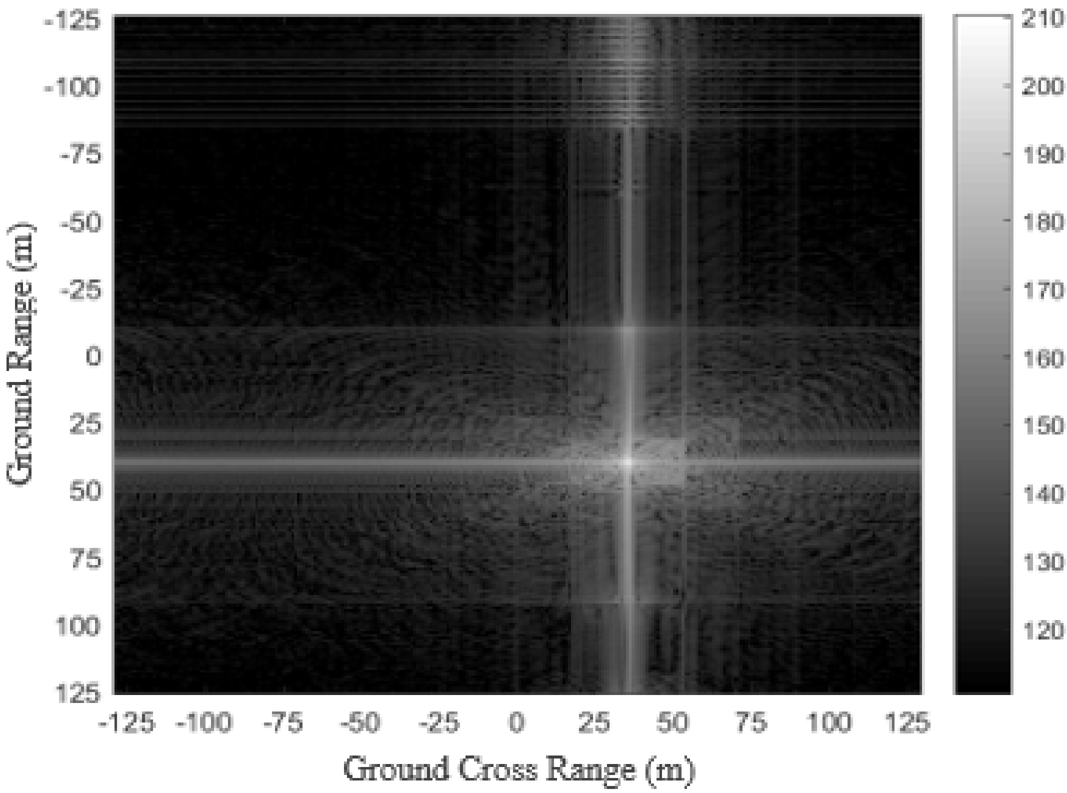

Figure 21. Length-100 Costas Code SAR Image of a Single Scattering Center Using the Parameters Defined in Table 1, Row 6

The range and cross-range profiles through the scattering center are shown in Figure 22 and Figure 23, respectively. The cross-range profile for the length-100 Costas code is similar to the length-15 Costas code; however, initial observation of the range profile appears to be distorted as there is no discernible sidelobe structure. This is the result of keeping the bandwidth of the waveform constant as the number of subpulses is increased. The length-15 Costas code analyzed previously has a subpulse length of 15.0 m. The length-100 Costas code waveform with a 300-MHz bandwidth has a subpulse bandwidth of 3.0 MHz, which is equivalent to a resolution of 100 m; therefore, only 2.5 lobes are expected across the length of the 250 m image. Because the scattering center is at 40 m, the lobes are calculated to be between -10 m to +90 m for the main lobe. A sidelobe starts at 90 m and extends past the end of the image. In addition, a sidelobe lies between -110 m to -10 m, and another sidelobe starts at -210 m and extends to -110 m. Inspection of Figure 22 reveals that the lobes approximately start and stop at the expected locations by identifying changes such as discontinuities in the range profile plot.

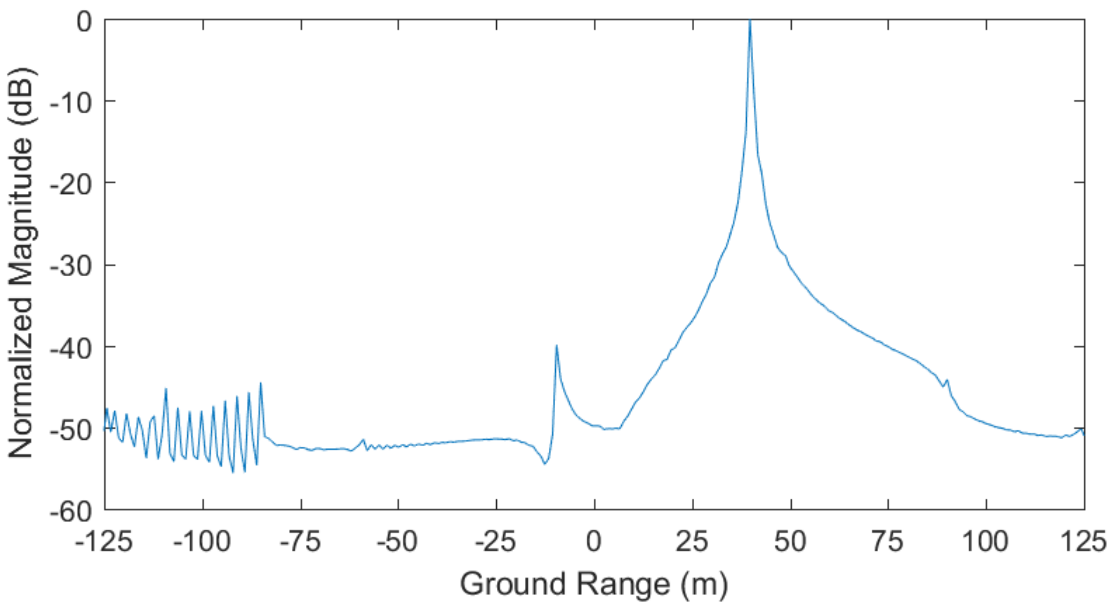

Figure 22. Length-100 Costas Code SAR Image Range Profile Slice of a Single Scattering Center Using the Parameters Defined in Table 1, Row 6

Five unique Costas codes were run through the SAR image generator in order to examine the dependence of image performance on a unique Costas codes. The resultant images are shown in Figure 25. In all of the images, the single scattering center is clearly visible and there are no major differences between the image. Closer inspection of the images reveals slight differences in the background generated by variations in the range sidelobe structure, as seen by the overlay of all five ground range profiles in Figure 24.

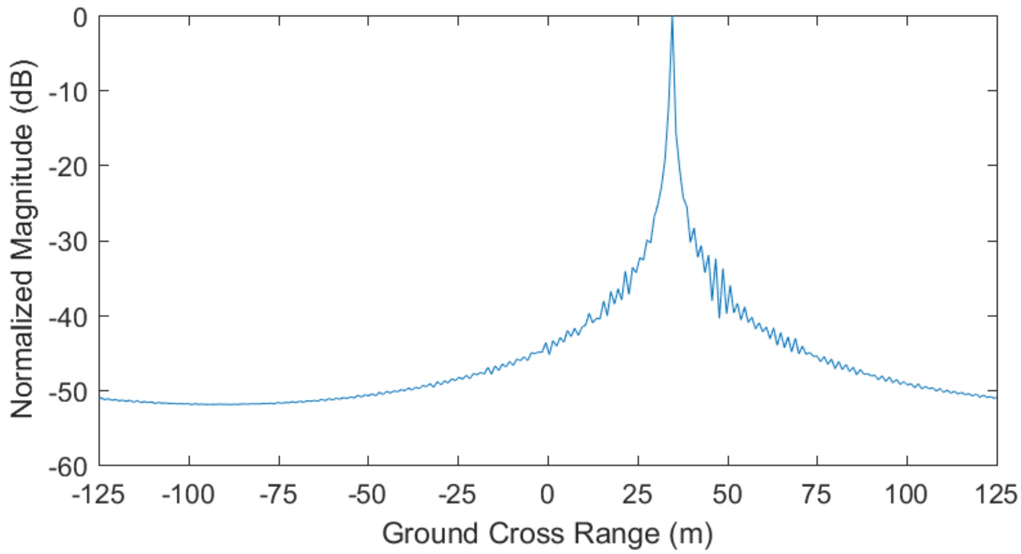

Figure 23. Length-100 Costas Code SAR Image Range Profile Slice of a Single Scattering Center Using the Parameters Defined in Table 1, Row 6

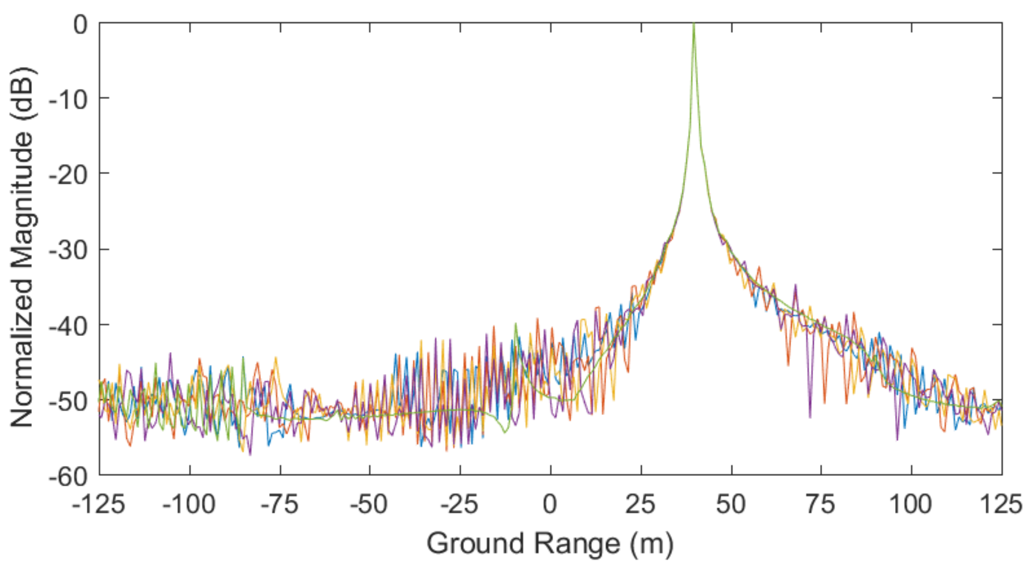

Figure 24. Overlay of Five Unique Length-100 Costas Code SAR Image Range Profile Slices for a Single Scattering Center Using the Parameters Defined in Table 1, Rows 6–10

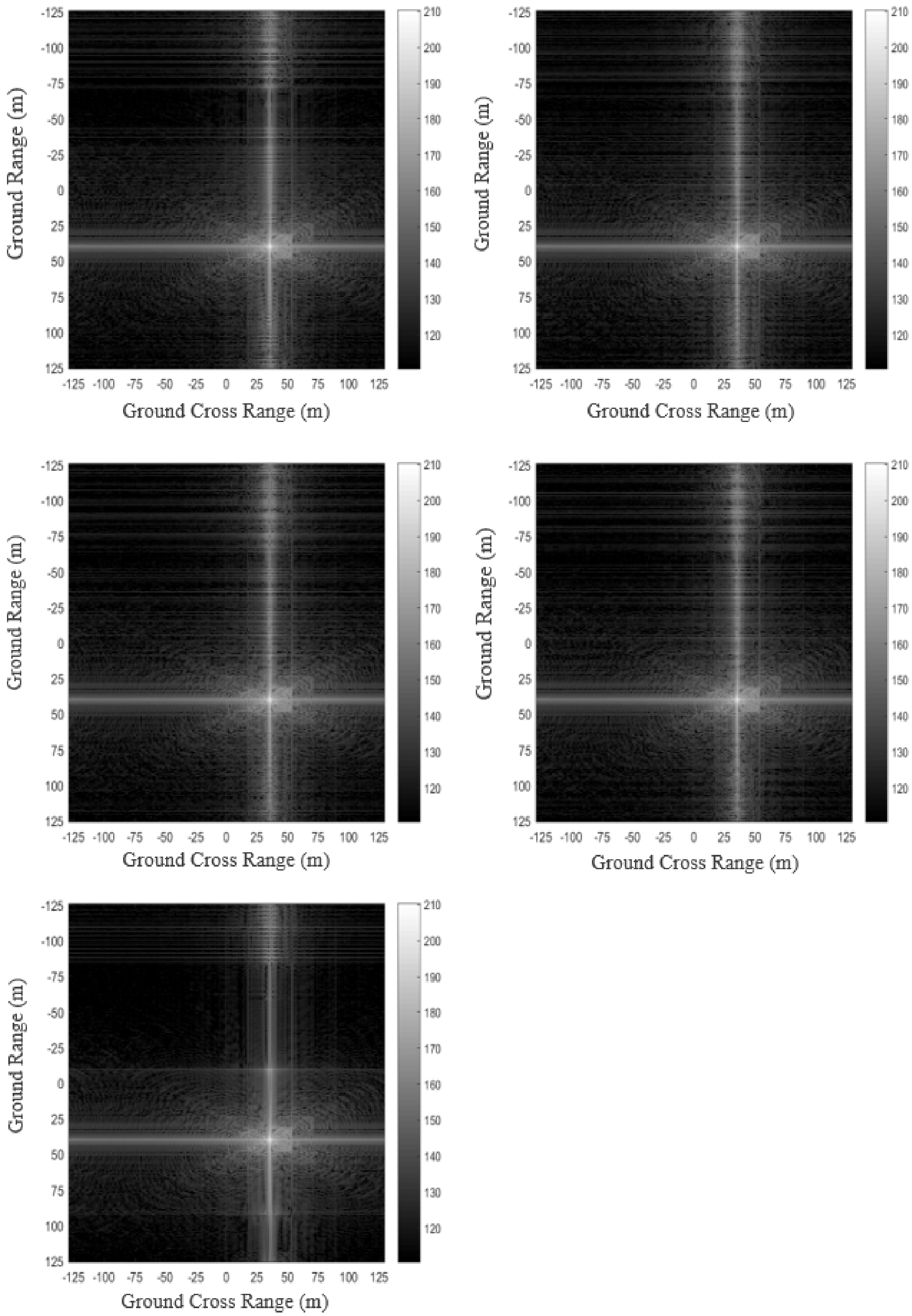

Figure 25. SAR Images Resulting from Five Unique Length-100 Costas Codes for a Single Scattering Center, as Defined in Table 1, Rows 6–10

3. Length-150 Costas Code

The length-150 Costas code from row 1 in Table 1 results in the single scattering center image shown in Figure 26. The scattering center is located in the expected position within the resolution tolerance.

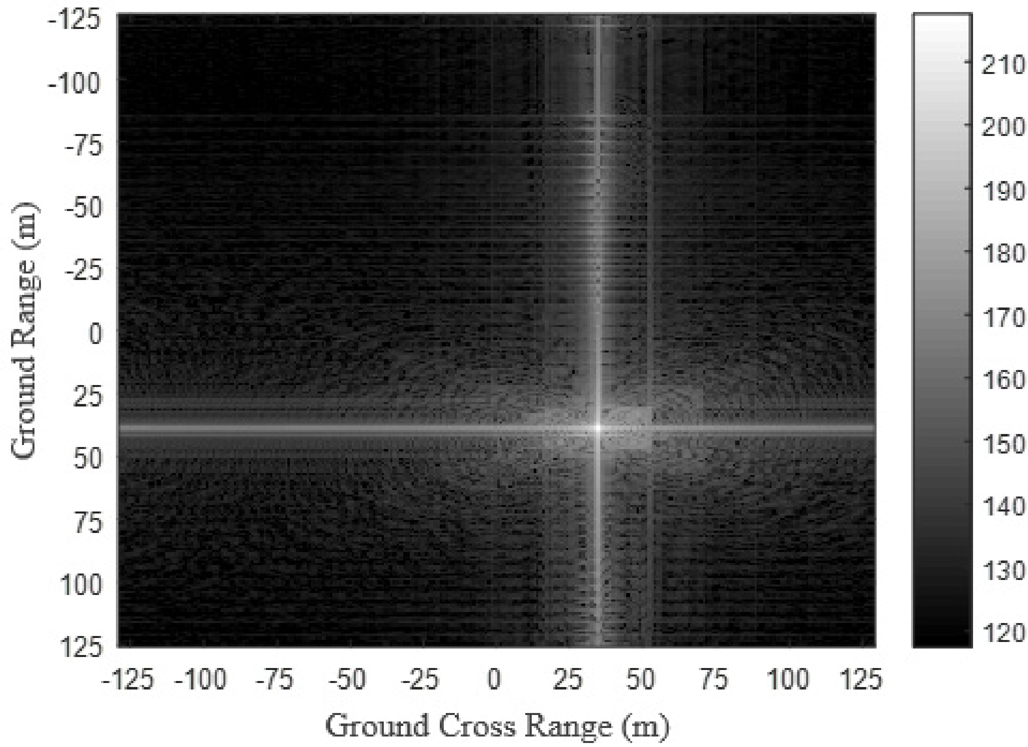

Figure 26. Length-150 Costas Code SAR Image for a Single Scattering Center Using the Parameters Defined in Table 1, Row 11

The range and cross-range profiles through the scattering center are shown in Figure 27 and Figure 28, respectively. The cross-range profile for the length-150 Costas code is similar to the length-15 and length-100 Costas codes. Again, the range profile appears to be distorted, as there is no periodic sidelobe structure. With the length-150 Costas code, the spacing of the sidelobes is greater than the total length of the range profile as a result of keeping the bandwidth of the waveform constant as the number of subpulses is increased. The length-150 Costas code has a 150-m resolution, which pushes most of the sidelobes outside of the image.

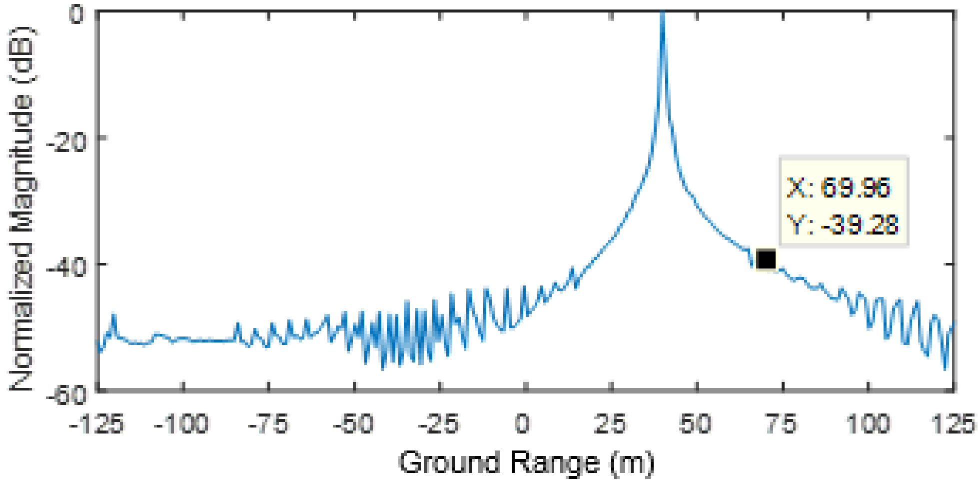

Figure 27. Length-150 Costas Code SAR Image Range Profile Slice for a Single Scattering Center Using the Parameters Defined in Table 1, Row 11

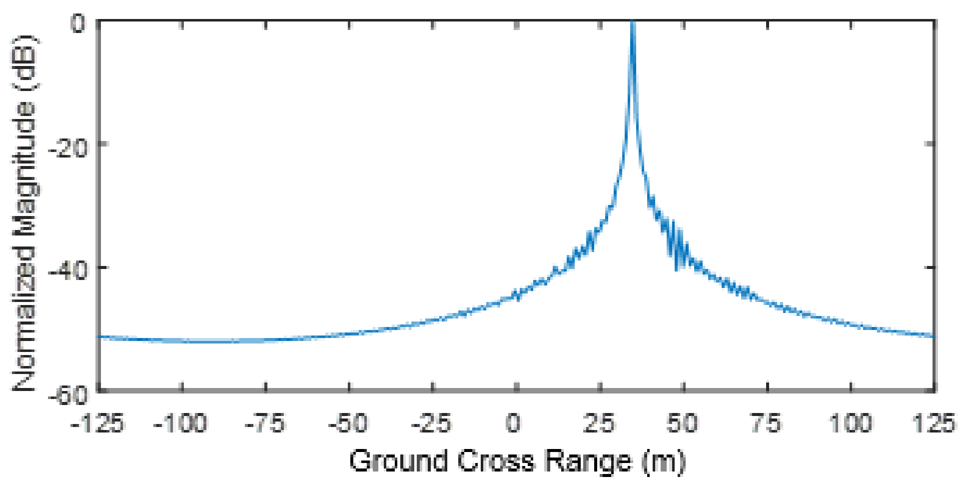

Figure 28. Length-150 Costas Code SAR Image Cross-Range Profile Slice for a Single Scattering Center Using the Parameters Defined in Table 1, Row 11

To examine the dependence of image performance on a unique Costas codes, five unique Costas codes were run through the SAR image generator. The resultant images are shown in Figure 29. In all of the images, the single scattering center is clearly visible, and there are no major differences between the images. Closer inspection of the images reveals slight differences in the background generated by variations in the range sidelobe structure, as seen by the overlay of all five ground range profiles in Figure 30.

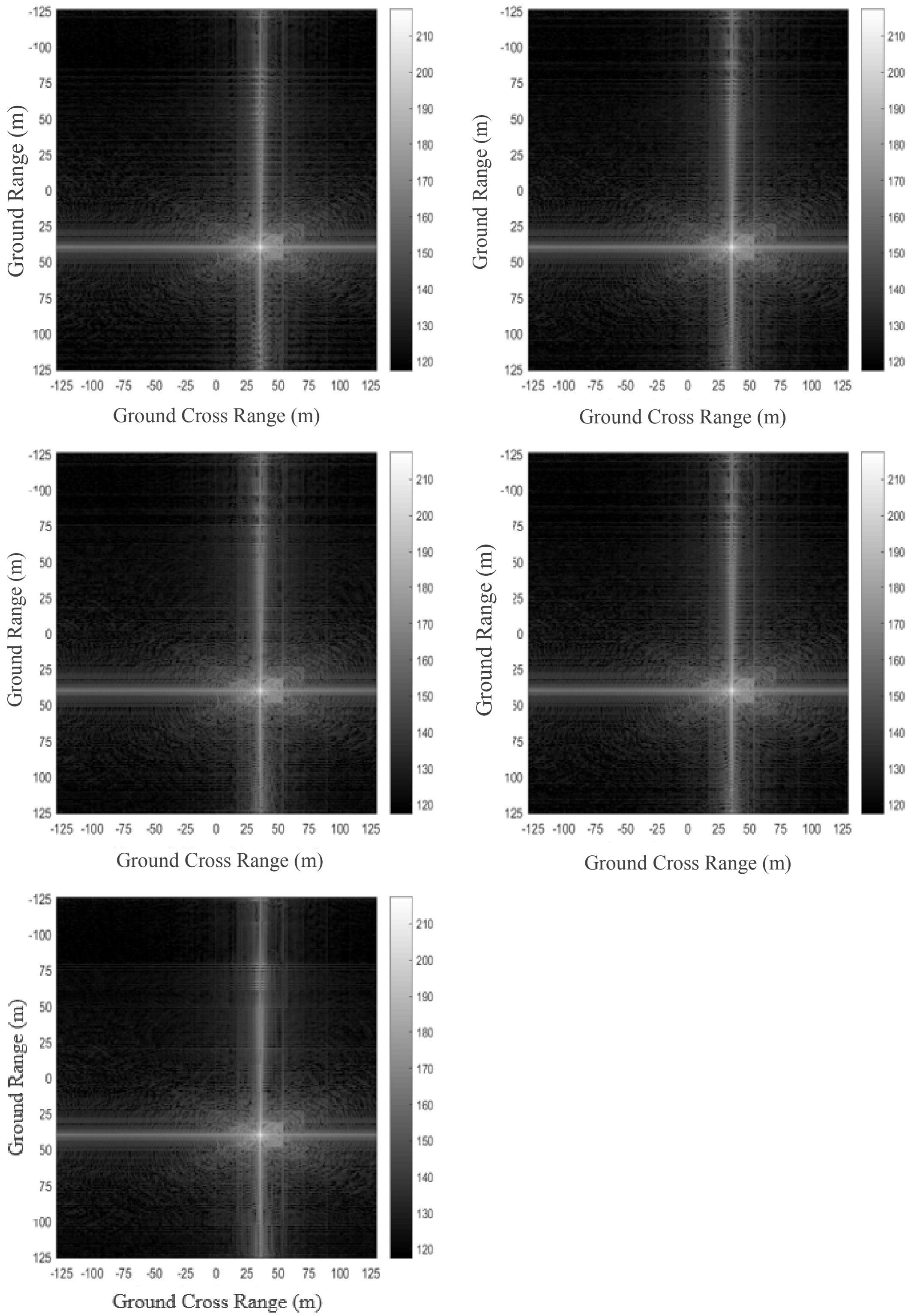

Figure 29. SAR Images Resulting from Five Unique Length-150 Costas Codes for a Single Scattering Center Using the Parameters Defined in Table 1, Rows 11–15

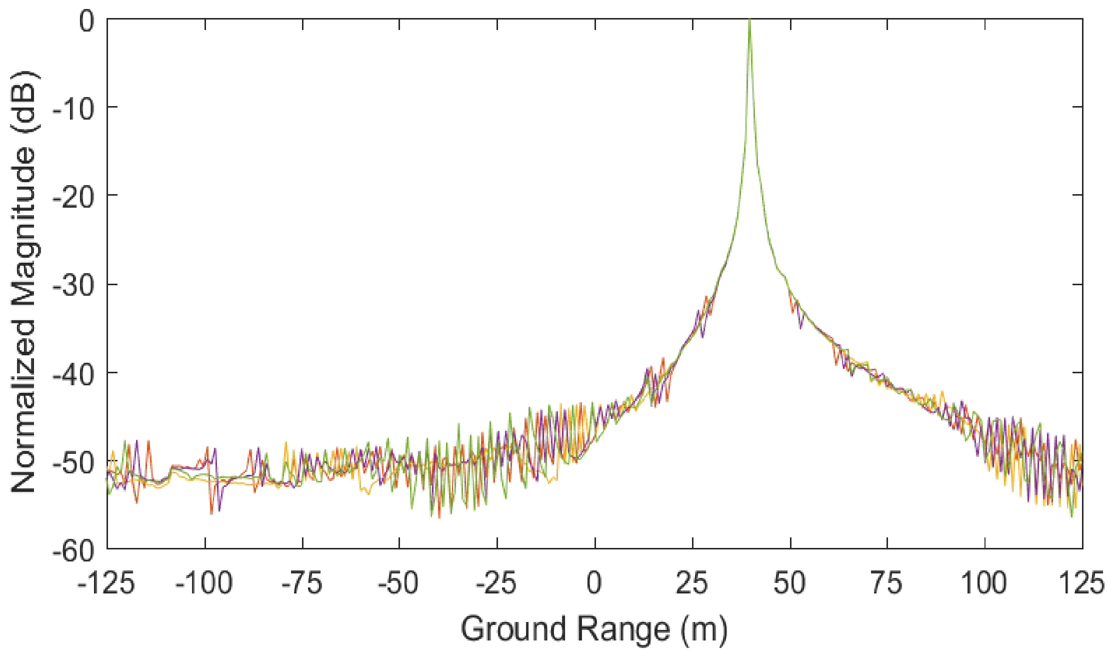

Figure 30. Overlay of Five Unique Length-150 Costas Code SAR Image Range Profile Slices for a Single Scattering Center Using the Parameters Defined in Table 1, Rows 11–15

4. Summary of Length-15, Length-100 and Length-150 Costas Codes for Generating SAR Images of a Single Scattering Center

A comparison between SAR images generated with three different length Costas codes is shown in Figure 31. In all three images, the point scattering center is clearly visible and is in the correct location. The size of the point target is identical in all images, which is expected since the bandwidth of the waveform is held constant as the length of the Costas code is varied.

When viewed side-by-side, the difference between the image produced with the length-15 Costas code in Figure 31 (a) and the length-100 and length-150 Costas codes in (b) and (c) are more apparent. The image produced by the length-15 Costas code has more visible sidelobe content than the images produced by the length-100 and length-150 Costas codes. The higher sidelobe levels produce stronger horizontal bands in the image which are less noticeable for the higher length Costas codes.

The differences between the images produced by the length-100 and length-150 Costas codes are subtle. Both appear to have the same amount of “black” space; although, the different sidelobe structures produce different background patterns in the images.

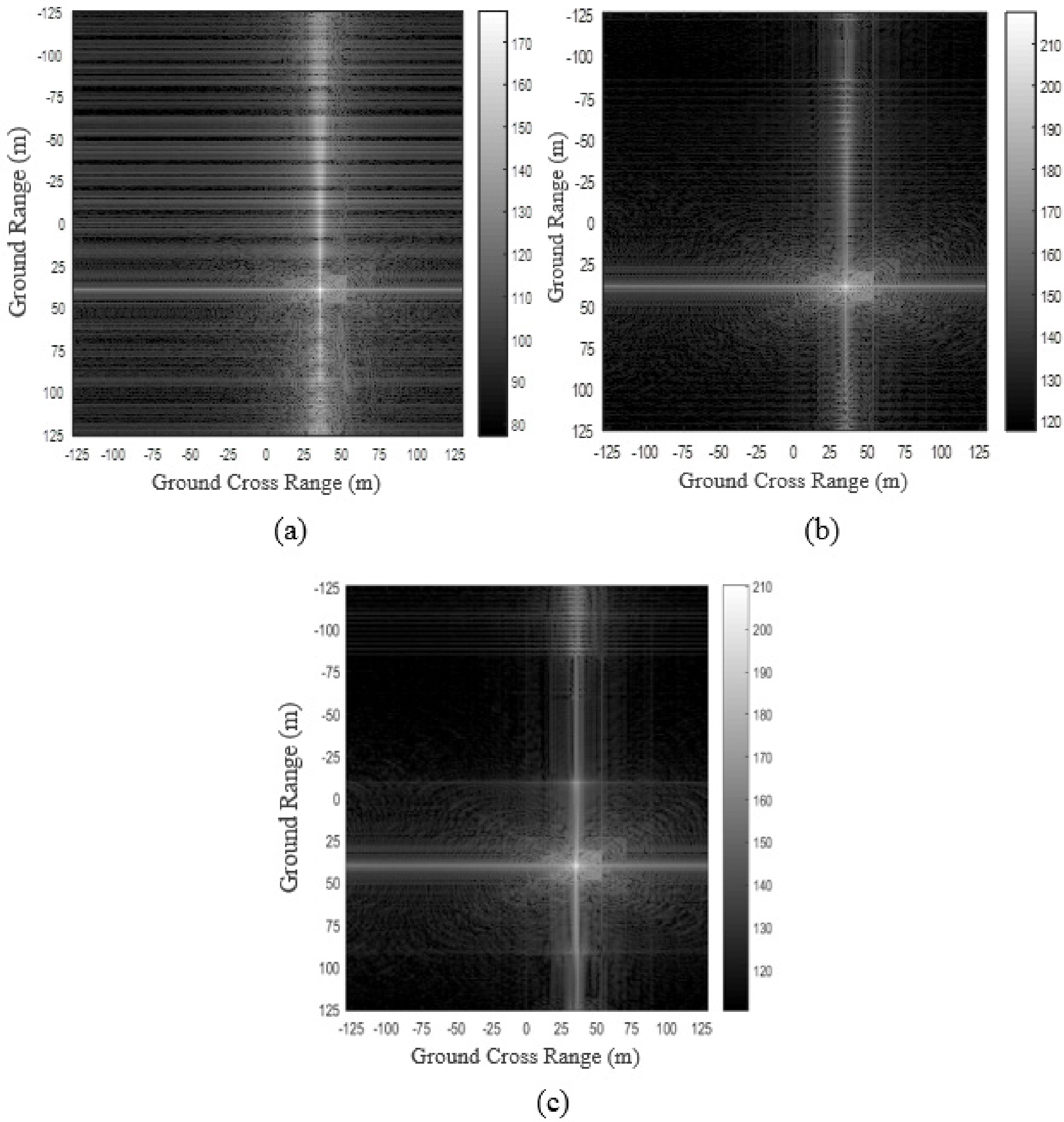

Figure 31. SAR Images Produced by Three Different Length Costas Codes: a Length-15 Costas Code (a), a Length-100 Costas Code (b), and a Length-150 Costas Code (c)

The impact of the code length on image performance is more evident when the range profile slice for each is overlaid, as seen in Figure 32. The range profile slices for the length-100 and length-150 Costas codes show the peak produced by the scatterer is in the same location and has the size and shape. The sidelobe levels for the length-100 and length-150 Costas codes are comparable. The length-15 Costas code does have a peak that is very close in size and shape to the higher-order Costas codes; however, the sidelobe levels for the length-15 Costas code are clearly larger in magnitude when compared to the length-100 and length-150 Costas codes.

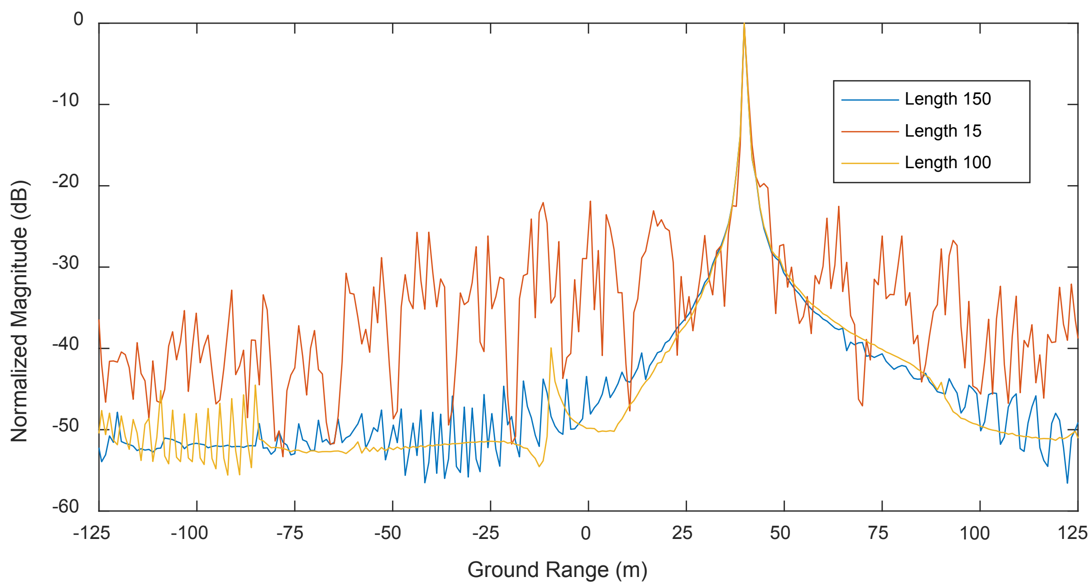

Figure 32. Overlay of Three Different Length Costas Code SAR Image Range Profile Slices Corresponding to Lengths of 15, 100, and 150 for a Single Scattering Center Using the Parameters Defined in Table 1, Rows 1, 6 and 11

B. DETAILED MULTIPLE SCATTERING CENTER ANALYSIS

1. Length-15 Costas Code

The first multiple scattering center image was generated using the parameters given in row 1 of Table 1. From the resultant image in Figure 33, we see that the point scattering centers are at the expected locations for the length-15 Costas code. The 100 dB of dynamic range of the image allows the sidelobe structure in both range and cross range to be clearly visible. The image slices through the scattering center in range and cross-range capture the sidelobe structures across the image.

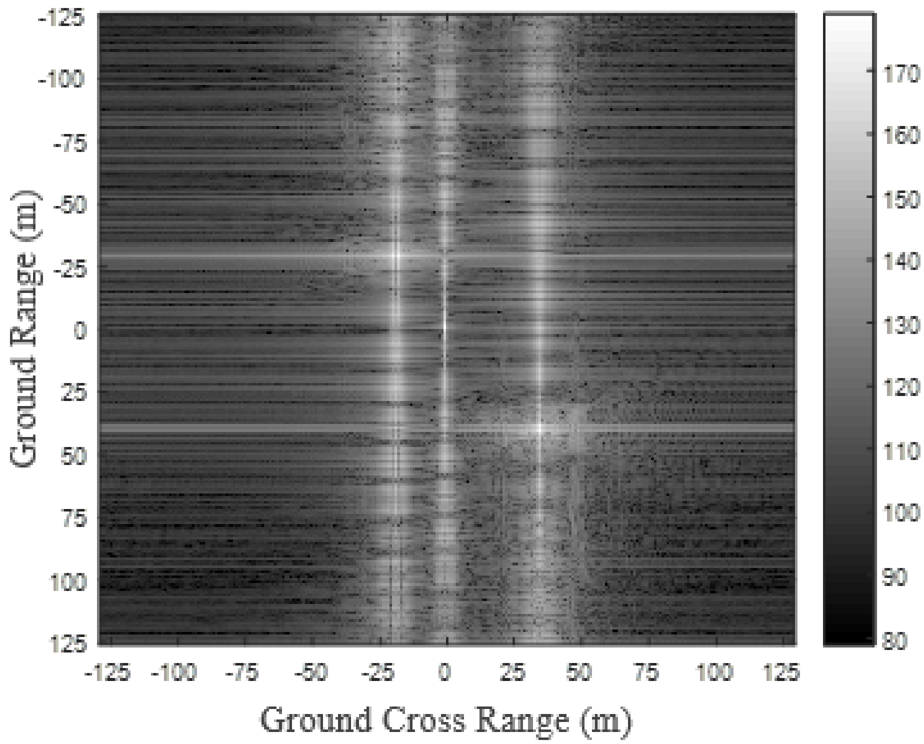

Figure 33. Length-15 Costas Code SAR Image with Multiple Scattering Centers Using the Parameters Defined in Table 1, Row 1

From the range plot in Figure 34, the positions of the four peaks in range are as expected. The two peaks spaced 2.0 m apart in range are clearly discernible as expected, due to the 1.0-m resolution. As with the single scattering center range profile, the sidelobes are down 20 dB or more from the peak lobe.

The four peaks are shown in the cross-range plot in Figure 35. The lack of sidelobe structure in cross-range as previously observed persists in the multiple scattering center scenario, so it is not surprising that the two scattering centers positioned 2.0 m apart in cross-range are clearly visible.

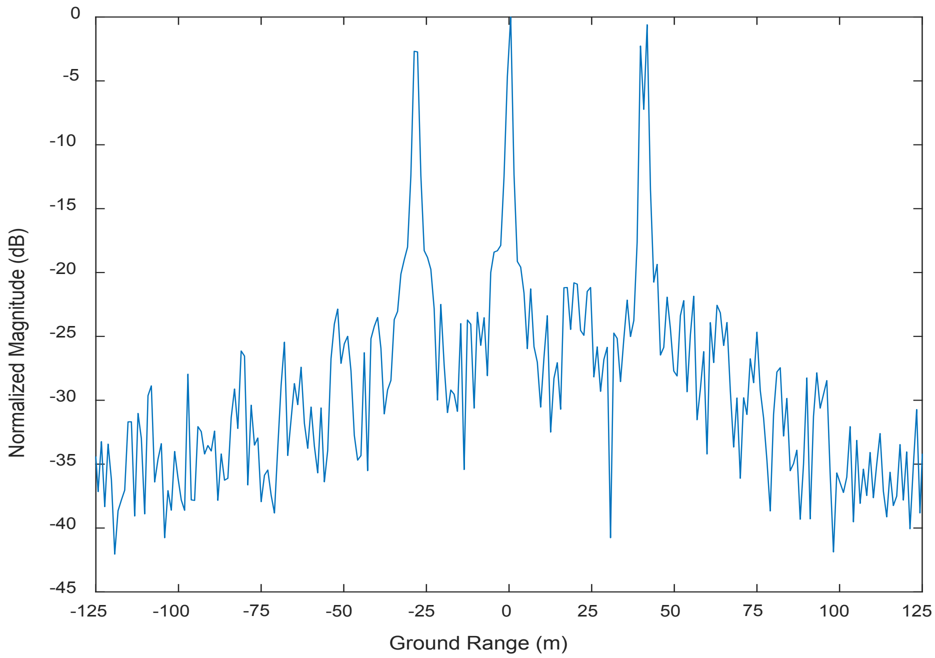

Figure 34. Length-15 Costas Code SAR Image Range Profile Slice for Multiple Scattering Centers Using the Parameters Defined in Table 1, Row 1

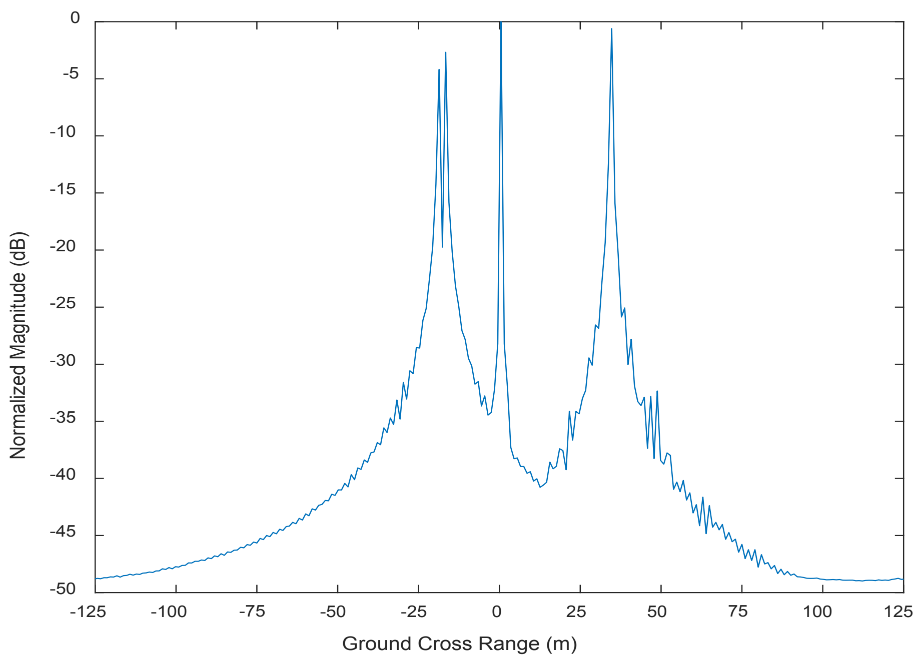

Figure 35. Length-15 Costas Code SAR Image Cross-Range Profile Slice for Multiple Scattering Centers Using the Parameters Defined in Table 1, Row 1

To examine the dependence of the multi-scattering center image performance on unique Costas codes, the five unique length-15 Costas codes used previously were executed through the SAR image generator. The slight differences in sidelobe structure between the five codes shown in the range profile of Figure 36 have no impact on the ability to detect the five scattering centers. The resultant images are shown in Figure 37 and reveal that the scattering centers are easily observable regardless of the particular code used.

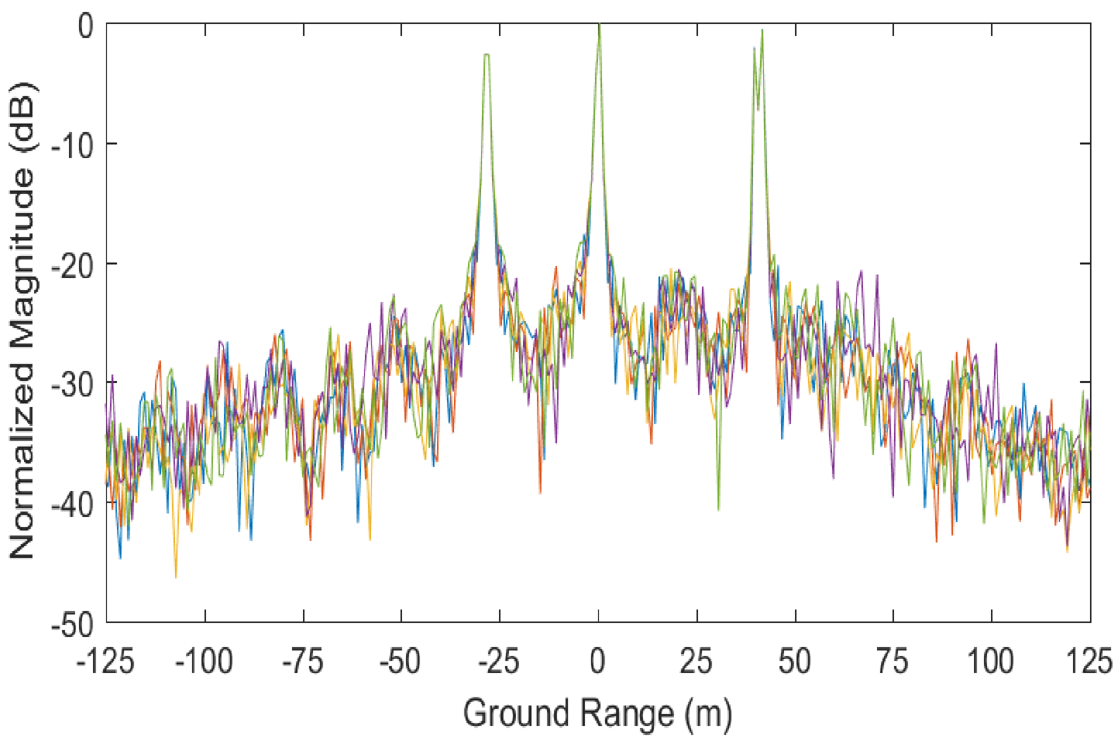

Figure 36. Overlay of Five Unique Length-15 Costas Code SAR Image Range Profile Slices for Multiple Scattering Centers Using the Parameters Defined in Table 1, Rows 1–5

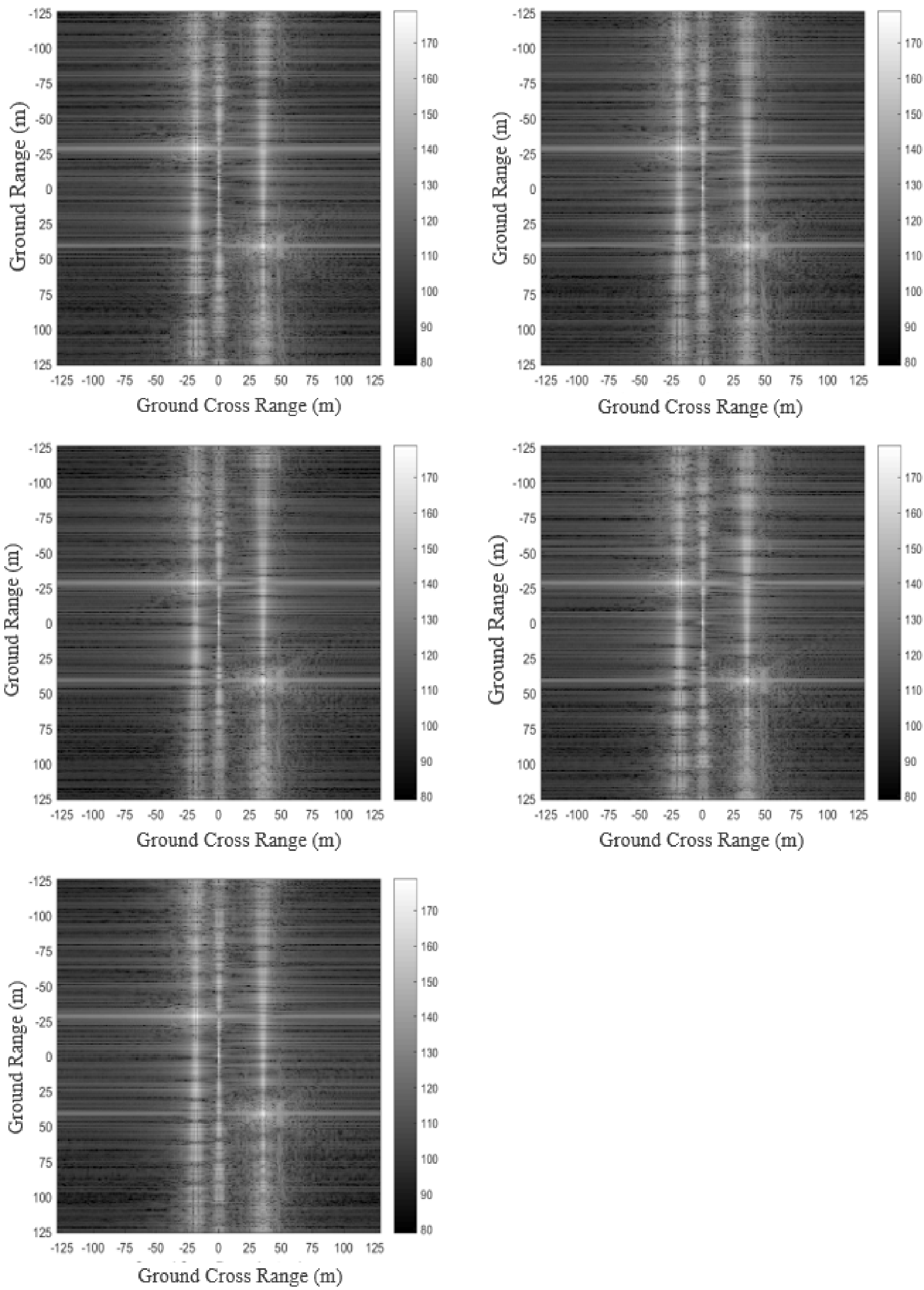

Figure 37. SAR Images Resulting from Five Unique Length-15 Costas Codes for Multiple Scattering Centers Using the Parameters Defined in Table 1, Rows 1–5

2. Length-100 Costas Code

The length-100 Costas code from row 6 in Table 1 results in the multiple scattering center image in Figure 38. The scattering centers are located in the expected positions within the 1.0-m resolution tolerance.

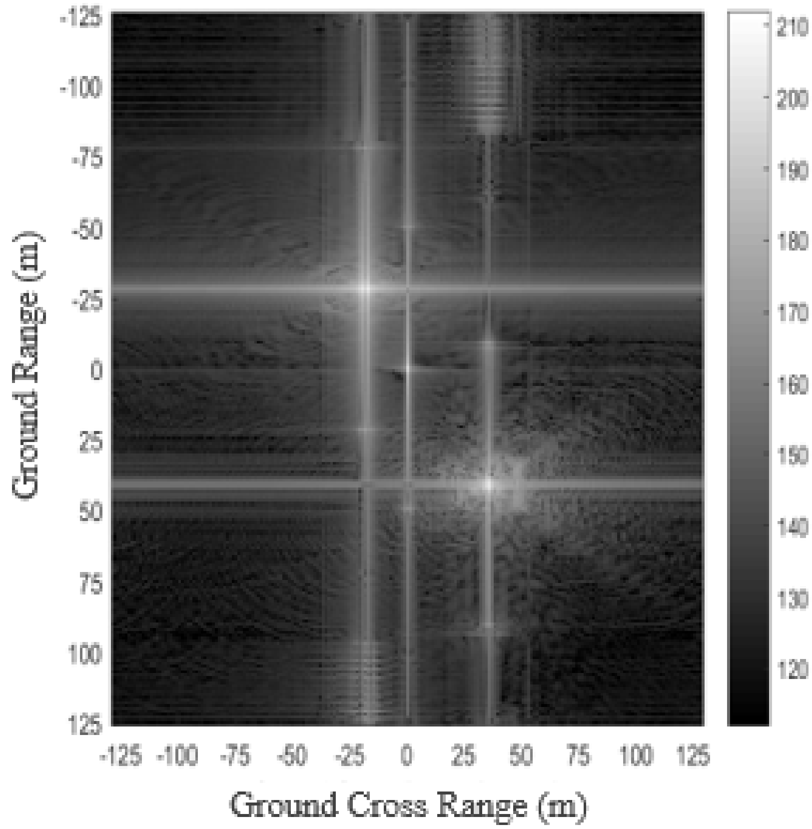

Figure 38. Length-100 Costas Code SAR Image with Multiple Scattering Centers Using the Parameters Defined in Table 1, Row 6

The range and cross-range profiles are shown in Figure 39 and Figure 40, respectively. The cross-range profile for the length-100 Costas code is similar to the length-15 Costas code. The scattering centers that are spaced 2.0 m apart in range and cross-range are distinguishable, as they were in the profiles for the length-15 Costas code. The longer Costas code results in lower sidelobe levels and has a greater potential dynamic range for generating images that do not include contributions from the sidelobes.

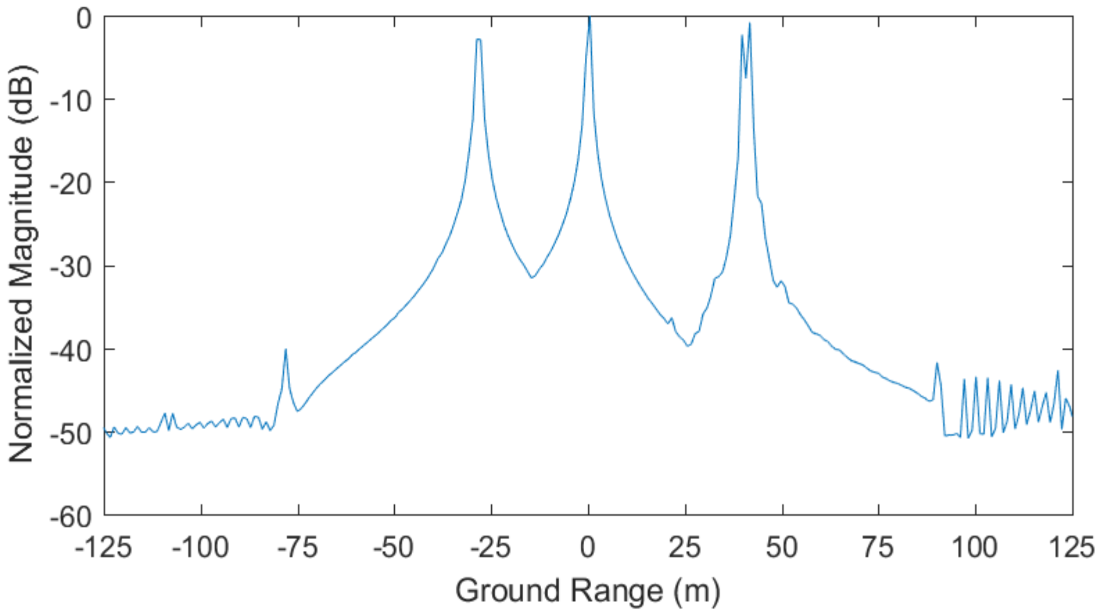

Figure 39. Length-100 Costas Code SAR Image Range Profile Slice for Multiple Scattering Centers Using the Parameters Defined in Table 1, Row 6

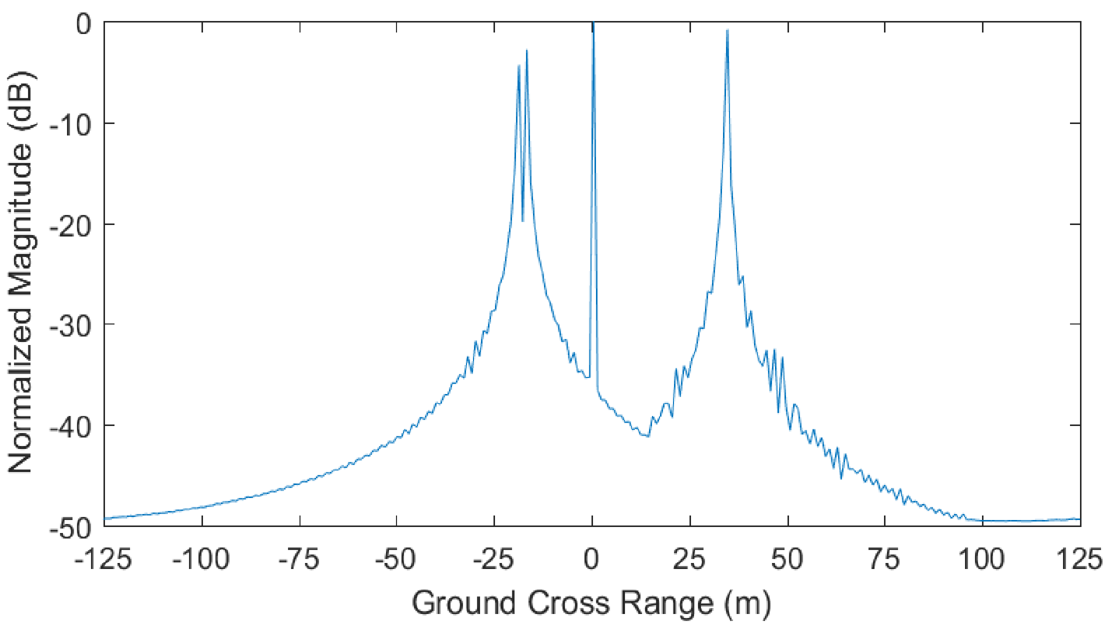

Figure 40. Length-100 Costas Code SAR Image Cross-Range Profile Slice for Multiple Scattering Centers Using the Parameters Defined in Table 1, Row 6

The five unique length-100 Costas codes used previously were executed through the SAR image generator in order to examine the dependence of the multi-scattering center image performance on unique Costas codes. The slight differences in sidelobe structure between the five codes shown in the range profile of Figure 41 have no impact on the ability to detect the five scattering centers. The resultant images are shown in Figure 42 and reveal that the scattering centers are easily observable regardless of the particular code used.

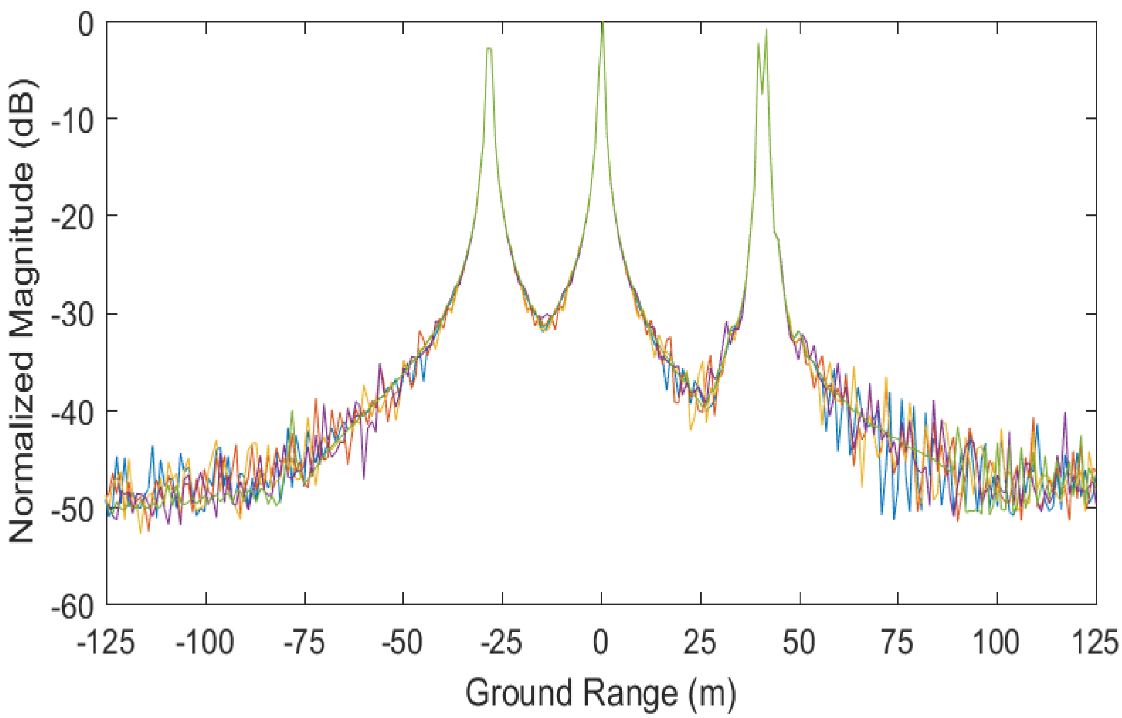

Figure 41. Overlay of Five Unique Length-100 Costas Code SAR Image Range Profile Slices for Multiple Scattering Centers Using the Parameters Defined in Table 1, Rows 6–10

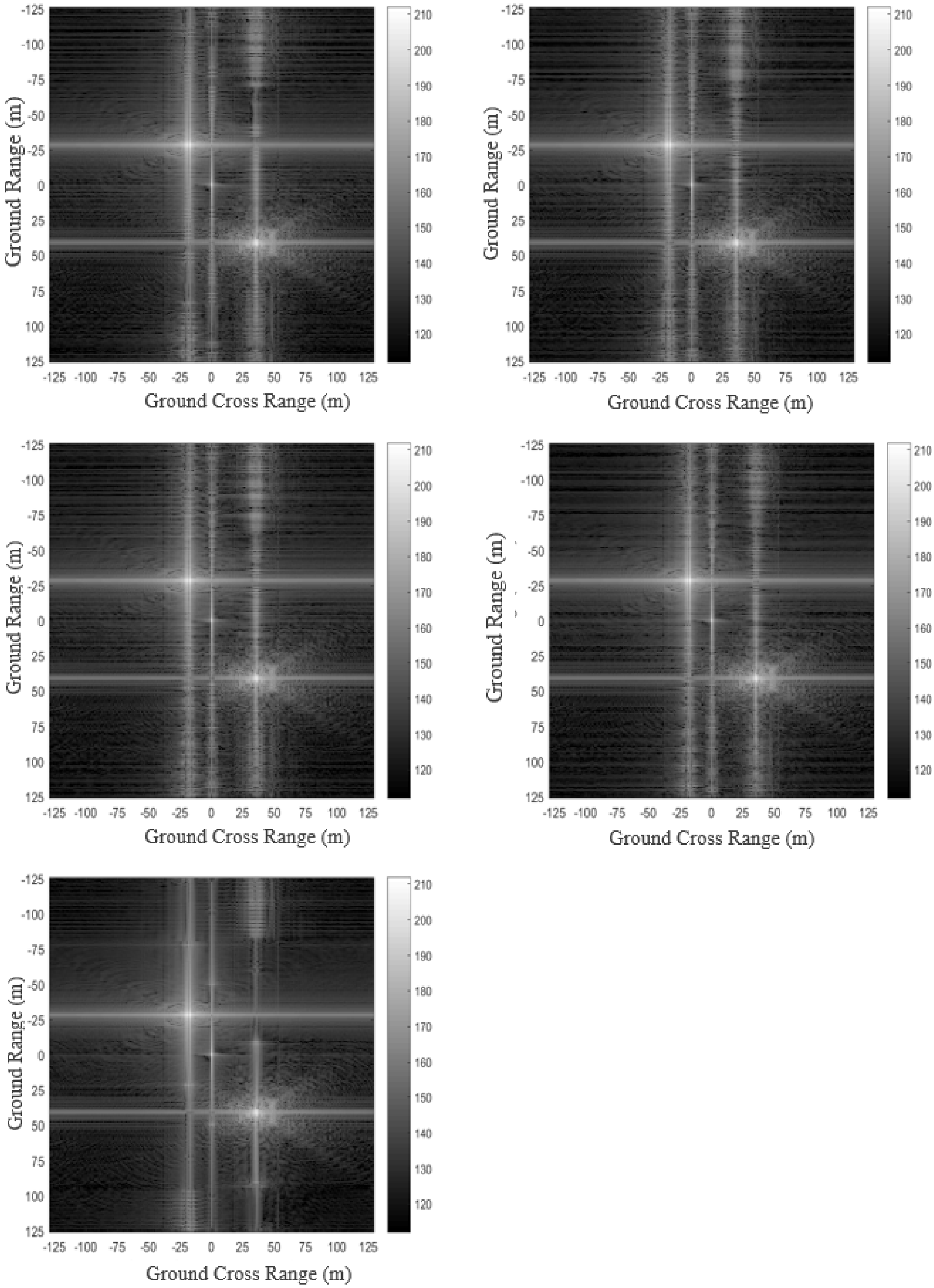

Figure 42. SAR Images of Five Unique Length-100 Costas Codes for Multiple Scattering Centers Using the Parameters Defined in Table 1, Rows 6–10

3. Length-150 Costas Code

The length-150 Costas code from row 11 in Table 1 results in the multiple scattering center image in Figure 43. The scattering center is located in the expected position within the resolution tolerance.

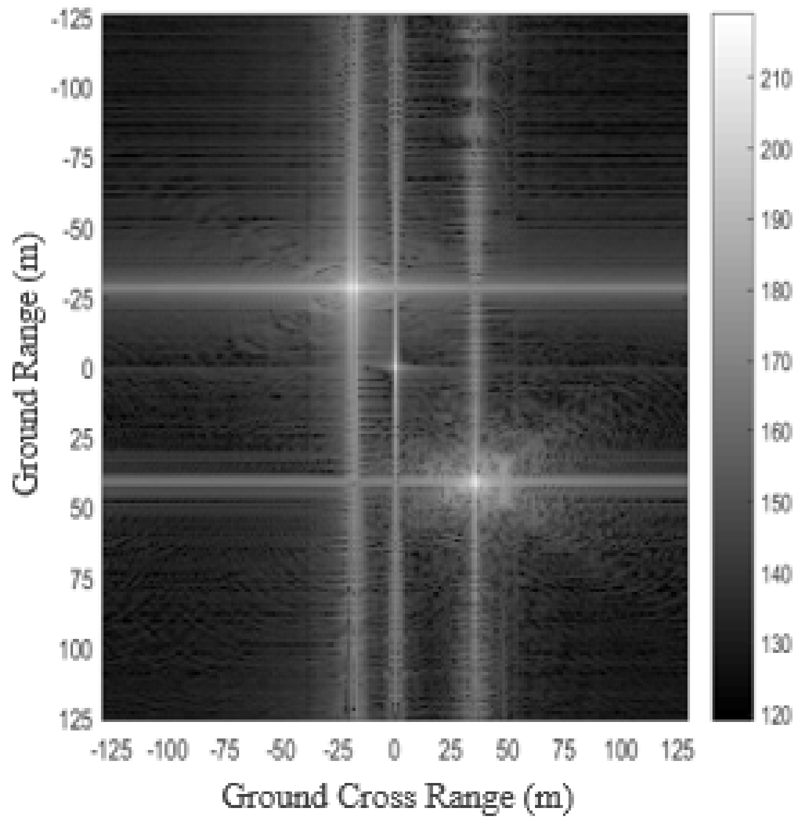

Figure 43. Length-150 Costas Code SAR Image with Multiple Scattering Centers Using the Parameters Defined in Table 1, Row 11

The range and cross-range profiles are shown in Figure 44 and Figure 45, respectively. The cross-range profile for the length-150 Costas code is similar to the length-100 Costas code. The scattering centers that are spaced 2.0 m apart in range and cross-range are distinguishable, as they were in the profiles for the length-100 Costas code. The longer Costas code results in lower sidelobe levels and has a greater potential dynamic range for generating images that do not include contributions from the sidelobes.

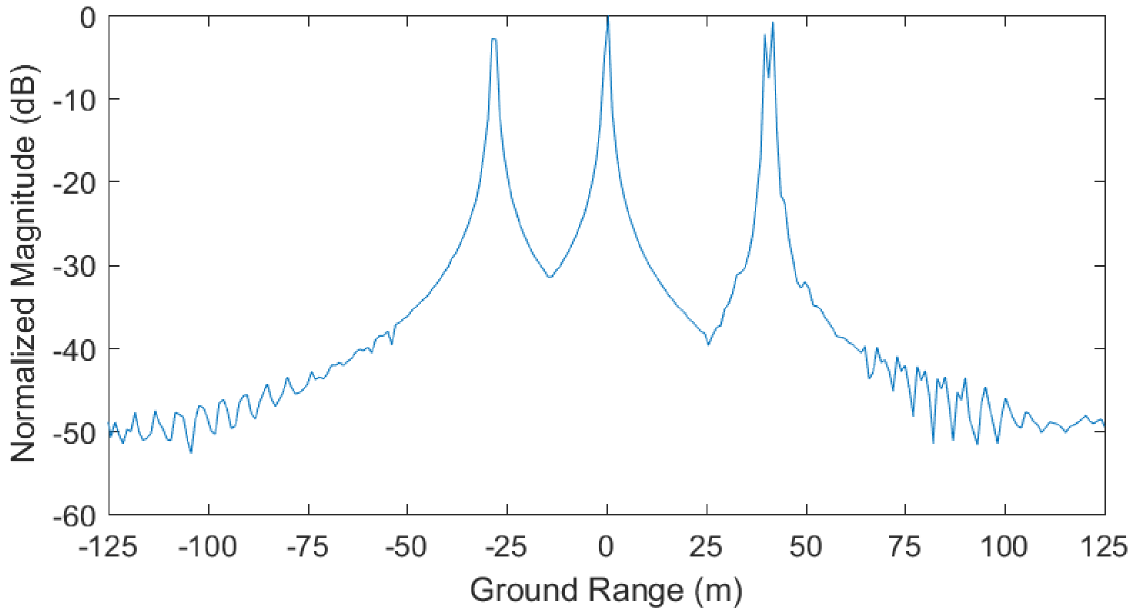

Figure 44. Length-150 Costas Code SAR Image Range Profile Slice for Multiple Scattering Centers Using the Parameters Defined in Table 1, Row 11

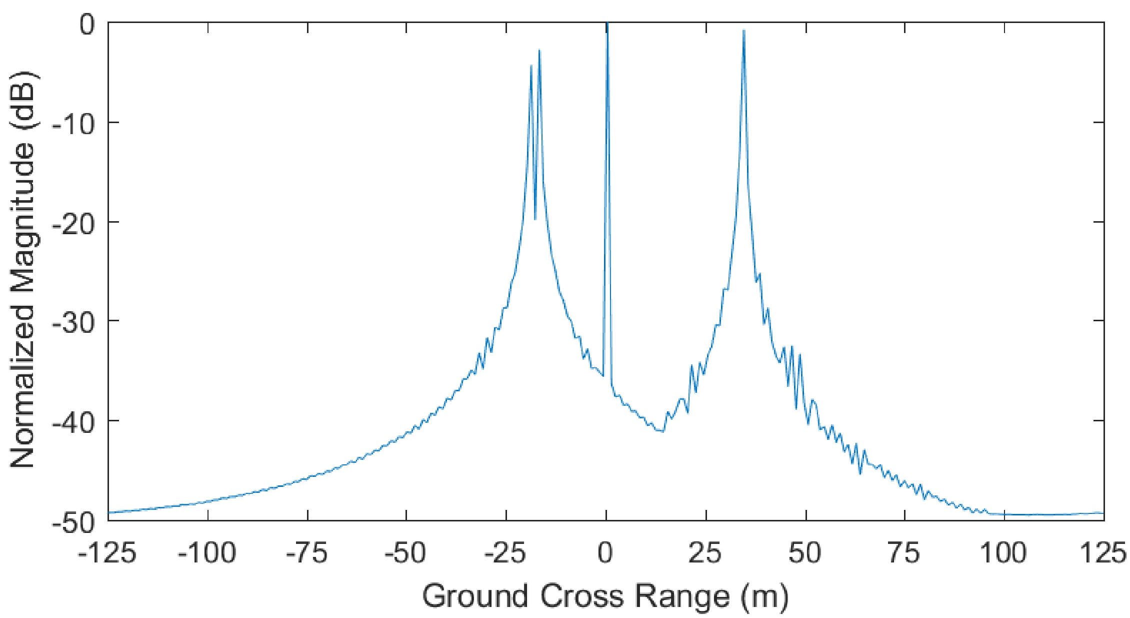

Figure 45. Length-150 Costas Code SAR Image Cross-Range Profile Slice for Multiple Scattering Centers Using the Parameters Defined in Table 1, Row 11

Five unique Costas codes were used to generate five images in order to confirm prior observations that the image quality is not dependent upon the unique Costas code used. A qualitative assessment of the images does not reveal any differences that affect the ability to clearly identify the five scattering centers. The slight differences in sidelobe structure between the five codes shown in the range profile of Figure 46 have no impact on the ability to detect the five scattering centers. The resultant images are shown in Figure 47 and reveal that the scattering centers are easily observable regardless of code used.

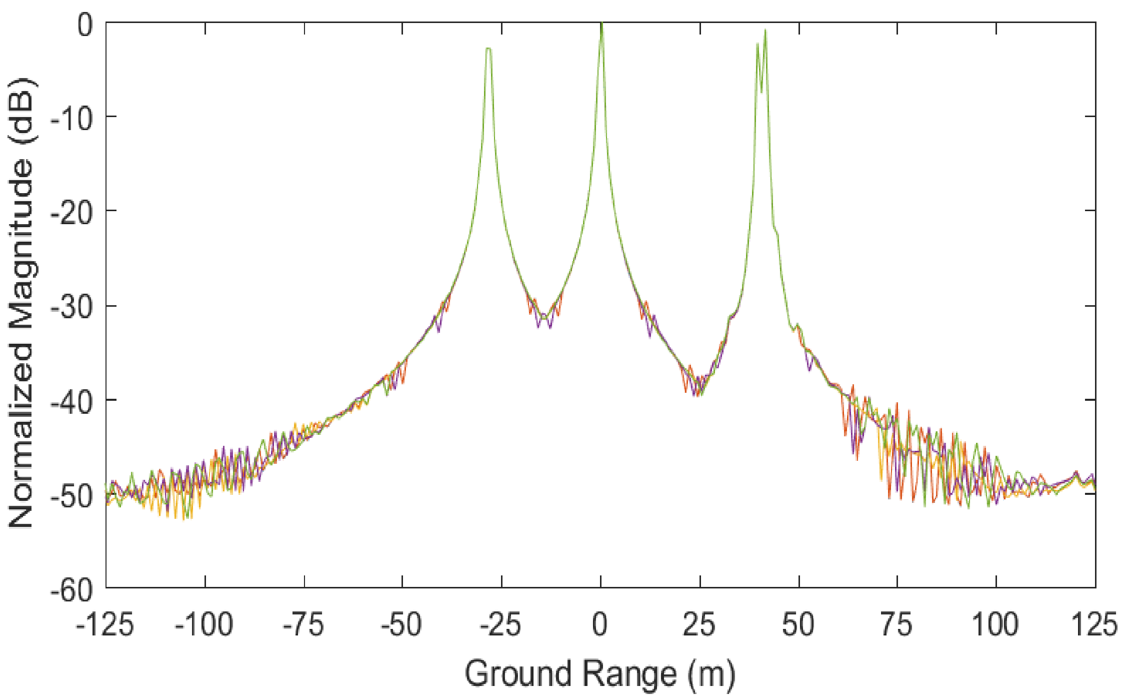

Figure 46. Overlay of Five Unique Length-150 Costas Code SAR Image Range Profile Slices for Multiple Scattering Centers Using the Parameters Defined in Table 1, Rows 11–15

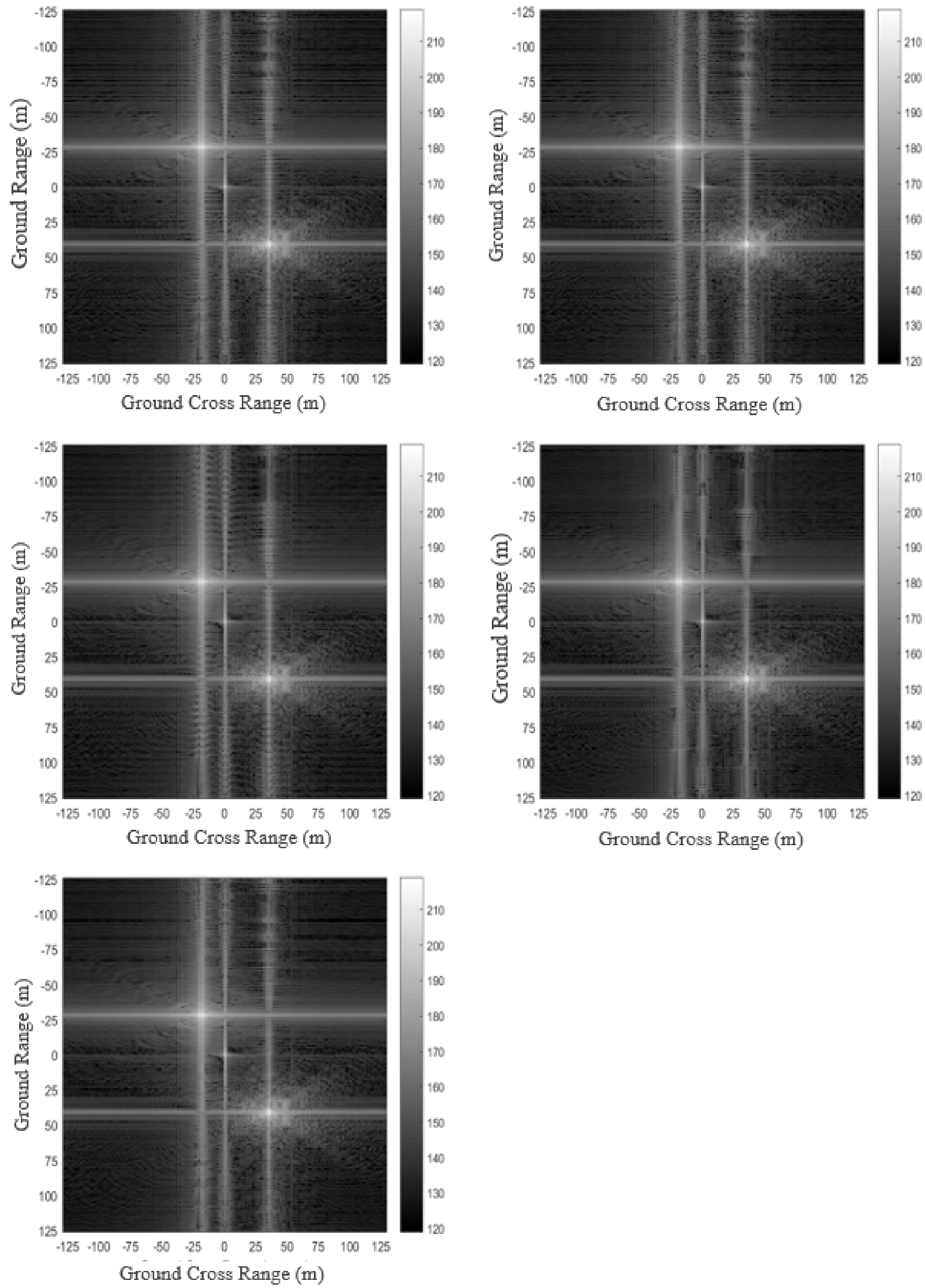

Figure 47. SAR Images of Five Unique Length-150 Costas Codes for Multiple Scattering Centers Using the Parameters Defined in Table 1, Rows 11–15

In this chapter, the images from the SAR simulations of three different length Costas Sequences were presented for scenes that included a single scattering center and a multiple scattering center. Simulation results for three unique sequences of each Costas sequence length were presented. In the next chapter, the conclusions from the SAR simulations are discussed along with recommendations for future work.

V. CONCLUSIONS AND RECOMMENDATIONS

A. SUMMARY AND CONCLUSIONS

In this thesis, we investigated the viability of using Costas-coded transmission waveforms to generate Spotlight Synthetic Aperture Radar images. Costas waveforms with sequence lengths of 15, 100, and 150 were used as the inputs to the SAR algorithm to evaluate the impact of longer sequences. To minimize the number of variables evaluated, the bandwidth of the waveforms was held constant. The results showed that the inherently low side lobe levels of Costas coded waveforms resulted in SAR images with easily discernible scattering centers. This is true for both images with a single scattering center and images with multiple scattering centers that were closely spaced in both range and cross-range. Increasing the sequence length of the Costas waveform increases the pulse-compression ratio of the waveform and results in images with improved peak-to-side-lobe ratios, yielding an effective higher dynamic range in the image. The sensitivity of the image fidelity due to specific sequences within specific sequence lengths was investigated but did not show a qualitative difference for the limited number of unique sequences simulated.

A no characteristic of the Costas waveform is that the improvement in image at higher sequence levels is obtained without increasing the overall bandwidth of the waveform. Since bandwidth can affect the cost of a system, this gives the designer of a SAR system the ability to improve the image quality while maintaining a cost-effective bandwidth.

The LPI nature of the Costas waveform is an additional feature that improves the performance of a SAR system in a contested RF environment. The wide bandwidth of the Costas waveform either requires a jammer to match the wide bandwidth, diluting their jamming power, or try to anticipate the frequency-hopping sequence to maximize the jammer power at the frequency of interest. This can easily be overcome by increasing the length of the Costas code such that it is virtually impossible for a jammer to extract the sequence.

B. FUTURE WORK

In this thesis, we showed that Costas coded waveforms are viable for use in SAR imaging systems. Additional work is required to understand the limits to the maximum length of the Costas-coded pulse due to range migration issues.

The longer Costas sequences have a large number of unique codes. Other work on Costas codes has identified some codes which are more optimal than others from a PSLR perspective. A next step is to identify those sequence lengths and specific codes that are better and quantify the improvement in SAR image quality.

Finally, other work has investigated modified Costas signals which use a combination of frequency and phase modulation or an increase of the frequency separation between subpulses beyond the orthogonality condition. A next step is to investigate the applicability of these modified Costas signals to further improve the LPI nature of the waveform or to further reduce the PSLR for improved SAR fidelity.

APPENDIX A. SPECIFIC CODES USED IN THE SIMULATIONS

Sequence Number	Costas Sequence Length	Code
1	5	1 , 3 , 4 , 2 , 5
2	5	2 , 4 , 3 , 1 , 5
3	5	4 , 1 , 3 , 2 , 5
4	5	4 , 5 , 2 , 1 , 3
5	5	5 , 3 , 2 , 4 , 1
6	100	1 , 2 , 4 , 8 , 16 , 32 , 64 , 27 , 54 , 7 , 14 , 28 , 56 , 11 , 22 , 44 , 88 , 75 , 49 , 98 , 95 , 89 , 77 , 53 , 5 , 10 , 20 , 40 , 80 , 59 , 17 , 34 , 68 , 35 , 70 , 39 , 78 , 55 , 9 , 18 , 36 , 72 , 43 , 86 , 71 , 41 , 82 , 63 , 25 , 50 , 100 , 99 , 97 , 93 , 85 , 69 , 37 , 74 , 47 , 94 , 87 , 73 , 45 , 90 , 79 , 57 , 13 , 26 , 52 , 3 , 6 , 12 , 24 , 48 , 96 , 91 , 81 , 61 , 21 , 42 , 84 , 67 , 33 , 66 , 31 , 62 , 23 , 46 , 92 , 83 , 65 , 29 , 58 , 15 , 30 , 60 , 19 , 38 , 76 , 51
7	100	23 , 38 , 54 , 98 , 17 , 72 , 97 , 90 , 96 , 62 , 19 , 27 , 49 , 59 , 36 , 99 , 45 , 48 , 31 , 60 , 64 , 75 , 80 , 18 , 100 , 73 , 24 , 66 , 30 , 32 , 88 , 40 , 9 , 50 , 87 , 12 , 33 , 15 , 16 , 44 , 20 , 55 , 25 , 94 , 6 , 67 , 58 , 8 , 22 , 10 , 78 , 63 , 47 , 3 , 84 , 29 , 4 , 11 , 5 , 39 , 82 , 74 , 52 , 42 , 65 , 2 , 56 , 53 , 70 , 41 , 37 , 26 , 21 , 83 , 1 , 28 , 77 , 35 , 71 , 69 , 13 , 61 , 92 , 51 , 14 , 89 , 68 , 86 , 85 , 57 , 81 , 46 , 76 , 7 , 95 , 34 , 43 , 93 , 79 , 91
8	100	49 , 10 , 68 , 18 , 82 , 93 , 87 , 26 , 96 , 67 , 92 , 60 , 4 , 7 , 88 , 53 , 17 , 55 , 71 , 99 , 47 , 57 , 24 , 42 , 23 , 15 , 1 , 27 , 22 , 89 , 80 , 39 , 43 , 50 , 37 , 90 , 6 , 61 , 31 , 29 , 76 , 32 , 56 , 98 , 20 , 35 , 36 , 63 , 85 , 73 , 52 , 91 , 33 , 83 , 19 , 8 , 14 , 75 , 5 , 34 , 9 , 41 , 97 , 94 , 13 , 48 , 84 , 46 , 30 , 2 , 54 , 44 , 77 , 59 , 78 , 86 , 100 , 74 , 79 , 12 , 21 , 62 , 58 , 51 , 64 , 11 , 95 , 40 , 70 , 72 , 25 , 69 , 45 , 3 , 81 , 66 , 65 , 38 , 16 , 28
9	100	70 , 35 , 68 , 34 , 17 , 59 , 80 , 40 , 20 , 10 , 5 , 53 , 77 , 89 , 95 , 98 , 49 , 75 , 88 , 44 , 22 , 11 , 56 , 28 , 14 , 7 , 54 , 27 , 64 , 32 , 16 , 8 , 4 , 2 , 1 , 51 , 76 , 38 , 19 , 60 , 30 , 15 , 58 , 29 , 65 , 83 , 92 , 46 , 23 , 62 , 31 , 66 , 33 , 67 , 84 , 42 , 21 , 61 , 81 , 91 , 96 , 48 , 24 , 12 , 6 , 3 , 52 , 26 , 13 , 57 , 79 , 90 , 45 , 73 , 87 , 94 , 47 , 74 , 37 , 69 , 85 , 93 , 97 , 99 , 100 , 50 , 25 , 63 , 82 , 41 , 71 , 86 , 43 , 72 , 36 , 18 , 9 , 55 , 78 , 39

10	**100**	100 , 99 , 97 , 93 , 85 , 69 , 37 , 74 , 47 , 94 , 87 , 73 , 45 , 90 , 79 , 57 , 13 , 26 , 52 , 3 , 6 , 12 , 24 , 48 , 96 , 91 , 81 , 61 , 21 , 42 , 84 , 67 , 33 , 66 , 31 , 62 , 23 , 46 , 92 , 83 , 65 , 29 , 58 , 15 , 30 , 60 , 19 , 38 , 76 , 51 , 1 , 2 , 4 , 8 , 16 , 32 , 64 , 27 , 54 , 7 , 14 , 28 , 56 , 11 , 22 , 44 , 88 , 75 , 49 , 98 , 95 , 89 , 77 , 53 , 5 , 10 , 20 , 40 , 80 , 59 , 17 , 34 , 68 , 35 , 70 , 39 , 78 , 55 , 9 , 18 , 36 , 72 , 43 , 86 , 71 , 41 , 82 , 63 , 25 , 50
11	**150**	1 , 6 , 36 , 65 , 88 , 75 , 148 , 133 , 43 , 107 , 38 , 77 , 9 , 54 , 22 , 132 , 37 , 71 , 124 , 140 , 85 , 57 , 40 , 89 , 81 , 33 , 47 , 131 , 31 , 35 , 59 , 52 , 10 , 60 , 58 , 46 , 125 , 146 , 121 , 122 , 128 , 13 , 78 , 15 , 90 , 87 , 69 , 112 , 68 , 106 , 32 , 41 , 95 , 117 , 98 , 135 , 55 , 28 , 17 , 102 , 8 , 48 , 137 , 67 , 100 , 147 , 127 , 7 , 42 , 101 , 2 , 12 , 72 , 130 , 25 , 150 , 145 , 115 , 86 , 63 , 76 , 3 , 18 , 108 , 44 , 113 , 74 , 142 , 97 , 129 , 19 , 114 , 80 , 27 , 11 , 66 , 94 , 111 , 62 , 70 , 118 , 104 , 20 , 120 , 116 , 92 , 99 , 141 , 91 , 93 , 105 , 26 , 5 , 30 , 29 , 23 , 138 , 73 , 136 , 61 , 64 , 82 , 39 , 83 , 45 , 119 , 110 , 56 , 34 , 53 , 16 , 96 , 123 , 134 , 49 , 143 , 103 , 14 , 84 , 51 , 4 , 24 , 144 , 109 , 50 , 149 , 139 , 79 , 21 , 126
12	**150**	36 , 134 , 29 , 66 , 145 , 28 , 121 , 140 , 1 , 96 , 5 , 27 , 25 , 135 , 125 , 71 , 21 , 53 , 105 , 114 , 72 , 117 , 58 , 132 , 139 , 56 , 91 , 129 , 2 , 41 , 10 , 54 , 50 , 119 , 99 , 142 , 42 , 106 , 59 , 77 , 144 , 83 , 116 , 113 , 127 , 112 , 31 , 107 , 4 , 82 , 20 , 108 , 100 , 87 , 47 , 133 , 84 , 61 , 118 , 3 , 137 , 15 , 81 , 75 , 103 , 73 , 62 , 63 , 8 , 13 , 40 , 65 , 49 , 23 , 94 , 115 , 17 , 122 , 85 , 6 , 123 , 30 , 11 , 150 , 55 , 146 , 124 , 126 , 16 , 26 , 80 , 130 , 98 , 46 , 37 , 79 , 34 , 93 , 19 , 12 , 95 , 60 , 22 , 149 , 110 , 141 , 97 , 101 , 32 , 52 , 9 , 109 , 45 , 92 , 74 , 7 , 68 , 35 , 38 , 24 , 39 , 120 , 44 , 147 , 69 , 131 , 43 , 51 , 64 , 104 , 18 , 67 , 90 , 33 , 148 , 14 , 136 , 70 , 76 , 48 , 78 , 89 , 88 , 143 , 138 , 111 , 86 , 102 , 128 , 57

13	150	63 , 4 , 41 , 5 , 89 , 44 , 149 , 55 , 73 , 31 , 129 , 1 , 48 , 39 , 60 , 11 , 75 , 127 , 56 , 121 , 70 , 38 , 12 , 123 , 15 , 116 , 132 , 145 , 14 , 68 , 93 , 85 , 3 , 144 , 117 , 29 , 33 , 74 , 79 , 17 , 61 , 59 , 114 , 36 , 67 , 45 , 46 , 94 , 133 , 42 , 53 , 128 , 104 , 9 , 130 , 49 , 87 , 99 , 71 , 86 , 51 , 32 , 26 , 40 , 108 , 50 , 135 , 138 , 131 , 97 , 126 , 8 , 82 , 10 , 27 , 88 , 147 , 110 , 146 , 62 , 107 , 2 , 96 , 78 , 120 , 22 , 150 , 103 , 112 , 91 , 140 , 76 , 24 , 95 , 30 , 81 , 113 , 139 , 28 , 136 , 35 , 19 , 6 , 137 , 83 , 58 , 66 , 148 , 7 , 34 , 122 , 118 , 77 , 72 , 134 , 90 , 92 , 37 , 115 , 84 , 106 , 105 , 57 , 18 , 109 , 98 , 23 , 47 , 142 , 21 , 102 , 64 , 52 , 80 , 65 , 100 , 119 , 125 , 111 , 43 , 101 , 16 , 13 , 20 , 54 , 25 , 143 , 69 , 141 , 124
14	150	111 , 41 , 150 , 121 , 89 , 80 , 134 , 51 , 39 , 19 , 47 , 10 , 40 , 64 , 128 , 131 , 113 , 119 , 21 , 99 , 23 , 127 , 146 , 90 , 67 , 120 , 78 , 144 , 27 , 58 , 143 , 61 , 86 , 43 , 112 , 49 , 65 , 101 , 79 , 29 , 30 , 103 , 13 , 57 , 17 , 76 , 55 , 20 , 7 , 147 , 2 , 50 , 12 , 8 , 25 , 74 , 60 , 107 , 81 , 138 , 22 , 73 , 62 , 141 , 18 , 16 , 108 , 123 , 35 , 42 , 34 , 129 , 84 , 145 , 106 , 31 , 70 , 9 , 54 , 109 , 117 , 110 , 48 , 33 , 91 , 93 , 66 , 137 , 148 , 97 , 63 , 6 , 32 , 135 , 149 , 100 , 83 , 87 , 125 , 77 , 72 , 82 , 95 , 130 , 1 , 92 , 132 , 88 , 28 , 105 , 104 , 4 , 26 , 140 , 124 , 37 , 118 , 11 , 136 , 68 , 133 , 102 , 69 , 3 , 45 , 142 , 15 , 71 , 52 , 98 , 24 , 96 , 44 , 38 , 56 , 53 , 139 , 115 , 85 , 122 , 94 , 114 , 126 , 59 , 5 , 14 , 46 , 75 , 116 , 36
15	150	150 , 145 , 115 , 86 , 63 , 76 , 3 , 18 , 108 , 44 , 113 , 74 , 142 , 97 , 129 , 19 , 114 , 80 , 27 , 11 , 66 , 94 , 111 , 62 , 70 , 118 , 104 , 20 , 120 , 116 , 92 , 99 , 141 , 91 , 93 , 105 , 26 , 5 , 30 , 29 , 23 , 138 , 73 , 136 , 61 , 64 , 82 , 39 , 83 , 45 , 119 , 110 , 56 , 34 , 53 , 16 , 96 , 123 , 134 , 49 , 143 , 103 , 14 , 84 , 51 , 4 , 24 , 144 , 109 , 50 , 149 , 139 , 79 , 21 , 126 , 1 , 6 , 36 , 65 , 88 , 75 , 148 , 133 , 43 , 107 , 38 , 77 , 9 , 54 , 22 , 132 , 37 , 71 , 124 , 140 , 85 , 57 , 40 , 89 , 81 , 33 , 47 , 131 , 31 , 35 , 59 , 52 , 10 , 60 , 58 , 46 , 125 , 146 , 121 , 122 , 128 , 13 , 78 , 15 , 90 , 87 , 69 , 112 , 68 , 106 , 32 , 41 , 95 , 117 , 98 , 135 , 55 , 28 , 17 , 102 , 8 , 48 , 137 , 67 , 100 , 147 , 127 , 7 , 42 , 101 , 2 , 12 , 72 , 130 , 25

THIS PAGE INTENTIONALLY LEFT BLANK

APPENDIX B. CRITICAL MATLAB CODE SEGMENTS

A. FUNCTION TO GENERATE A COSTAS WAVEFORM

```
function [waveformWithNoise,waveformWithOutNoise] =
CostasFunction(Costas_Props)
% clear all;
% clc;
% disp('*******************************************');
% disp('**************COSTAS CODE ****************');
% disp('*******************************************');

%DEFAULT VARIABLE
A = Costas_Props.A;                               % Amplitude of signal
fs = Costas_Props.fs;                             % Sampling frequency
SNR_dB = Costas_Props.SNR_dB;                     % Signal to noise ratio
tp = Costas_Props.tp;                             % Sub-period (s)
BW=Costas_Props.subPulseBandWidth;                % bandwidth (hopping
frequency delta)
CF=Costas_Props.CF;                                  % Center Frequency
StartFreq = Costas_Props.StartFreq;
NumberCodePeriods=Costas_Props.NumberCodePeriods;             % Number
of code periods

seq=Costas_Props.Sequence;
seq=seq(seq~=0);
seq=seq-1;
[a,length]=size(seq);

seq=seq*BW; %

tb=1/(fs); % Sampling period

% This section generates I & Q without COSTAS phase shift and I & Q
      with Phase shift. The signals are generated
% five times by the outer loop. The variable 'index' is used to
      generate a time vector for time domain plots.
f3s=figure;
f4s=figure;

index=0;
waveform_segment_prev = 0;
numseq=NumberCodePeriods;
totalPhaseDiscontinuities = 0;
phaseCorrection = 1;
%Generate the signal five times and store sequentially in corresponding
vectors
    for xx=1:length
            Ntp = ceil(fs*tp);
            ExtendedNtp=Ntp*2;
            I_CostasSegment=A*cos(2*pi*seq(xx)*(0:ExtendedNtp)*tb);
```

```
Q_CostasSegment=A*sin(2*pi*seq(xx)*(0:ExtendedNtp)*tb);
[waveformSegment] = I_CostasSegment+(Q_CostasSegment*1i);

if xx>1
    waveformNoPhaseCorrection = [waveformNoPhaseCorrection
      waveformSegment(1:Ntp)];
    phaseTestSegment = [waveform waveformSegment];
    deltaPhase=abs(phaseTestSegment(2:end)-
      phaseTestSegment(1:end-1));
    deltaDeltaPhase = deltaPhase(2:end)-deltaPhase(1:end-
      1);

    numPhaseDiscontinuities = sum(abs(deltaDeltaPhase) >
      10e-10);
    shiftIndex = 1;
    bestIndex = 0;
    halfwayIndex = 0;
    minDeltaPhaseValue = 100;
    while numPhaseDiscontinuities >
      totalPhaseDiscontinuities+1
        shiftIndex = shiftIndex+1;
        if shiftIndex == (ExtendedNtp-Ntp)
            if halfwayIndex ~= 0
                bestIndex = halfwayIndex;
            else
                bestIndex = testIndex;
            end
            break
        end

        waveformtest = [waveform
            waveformSegment(shiftIndex:end)];

        deltaPhase=abs(waveformtest(2:end)-
            waveformtest(1:end-1));
        deltaDeltaPhase = deltaPhase(2:end)-
            deltaPhase(1:end-1);
        if deltaPhase((xx-1)*Ntp)> deltaPhase(((xx-1)*Ntp)-
            1)
            if deltaPhase((xx-1)*Ntp)< deltaPhase(((xx-
            1)*Ntp)+1)
                halfwayIndex = shiftIndex;
            end
        end
        if abs(deltaDeltaPhase((xx-1)*Ntp)) <
            minDeltaPhaseValue
            minDeltaPhaseValue = abs(deltaDeltaPhase((xx-
                  1)*Ntp));
            testIndex = shiftIndex;
        end

        %figure(f3s);plot(deltaPhase);
```

```
                numPhaseDiscontinuities = sum(abs(deltaDeltaPhase)
                    > 10e-10);
            end

            if bestIndex ~= 0
                waveformtest = [waveform
                    waveformSegment(bestIndex:bestIndex+Ntp-1)];
            else
                waveformtest = [waveform
                    waveformSegment(shiftIndex:shiftIndex+Ntp-1)];
            end

        else
            waveformtest = waveformSegment(1:Ntp);
            waveformNoPhaseCorrection = waveformSegment(1:Ntp);
            numPhaseDiscontinuities=0;
        end
        totalPhaseDiscontinuities = numPhaseDiscontinuities;
        waveform = waveformtest;

    end
for p=1:numseq %Generate the signal N times and store sequentially in
corresponding vectors
    waveform = [waveform waveformtest];
end

if phaseCorrection == 0
    waveform = waveformNoPhaseCorrection;
end


I = real(waveform);
Q = imag(waveform);


%Power Spectral Density for I with phase shift & with WGN with Signal
to noise ratios
%for loop makes calculations and plots for each value of SNR for WGN
[a,b]=size(I);
samps_seq=b/numseq; %Samples in a sequence

SNR=10^(SNR_dB/10);
power=10*log10(A^2/(2*SNR));%calculate SNR in dB for WGN function
noise=wgn(a,b,power);%calculate noise at specified SNR
IN=I+noise;                 %add noise to I with COSTAS phase shift
IPWON=I;                  %I with phase shift without noise
QN=Q+noise;              %add noise to Q with COSTAS phase shift
QPWON=Q;                %Q with phase shift without noise

% This section generates the files for analysis

INP=IN';%transpose I with noise and COSTAS phase shift for text file
QNP=QN';%transpose Q with noise and COSTAS phase shift for text file
```

```
IPWONT=IPWON';%transpose I with phase without noise for text file
QPWONT=QPWON';%transpose Q with phase without noise for text file

% % save results in data files

I= INP(:,1);
Q=QNP(:,1);

II= IPWONT(:,1);
QQ=QPWONT(:,1);
waveformWithNoise = [I(:,1)+(Q(:,1)*1i)];

[w1,w2] = size(waveformWithNoise);
code_length = w1/NumberCodePeriods;

waveformWithOutNoise = II(1:code_length)+1i*QQ(1:code_length);

option2 = 1;
ffs=floor(fs/1e6); %sample frequency in MHz
tpp=numel(I); %number of samples in 1 waveform
save(['C_' num2str(option2) '_' num2str(NumberCodePeriods) '_'
num2str(ffs) '_' num2str(tpp) '_' num2str(CF/1e9) '_'
num2str(BW*length/1e6) '_' num2str(SNR_dB)],'I','Q');
save(['C_' num2str(option2) '_' num2str(NumberCodePeriods) '_'
num2str(ffs) '_' num2str(tpp) '_' num2str(CF/1e9) '_'
num2str(BW*length/1e6) '_s'],'I','Q');
disp(' ');
disp(['Signal and noise save as :  C_' num2str(option2) '_'
num2str(NumberCodePeriods) '_' num2str(ffs) '_' num2str(tpp) '_'
num2str(CF/1e9) '_' num2str(BW*length/1e6) '_' num2str(SNR_dB)]);
disp(['Signal only save as :         C_' num2str(option2) '_'
num2str(NumberCodePeriods) '_' num2str(ffs) '_' num2str(tpp) '_'
num2str(CF/1e9) '_' num2str(BW*length/1e6) '_s']);
disp(['Directory:                              ' num2str(cd)]);
disp(['NOTE: Number of sequences = ' num2str(numseq) ' Samples in
single FH sequence = ' num2str(samps_seq)]);

figure(f3s);plot(deltaPhase);
figure(f4s);plot(deltaDeltaPhase);
```

B. CODE SNIPPET TO PROCESS THE WAVEFORM RESPONSE AGAINST THE SCATTERING CENTERS

```
% Recreate waveform
[w1,w2] = size(waveform);
% Recreate Reference waveform
[CR1,CR2] = size(Correlation_Ref);
code_length = sensor_props.code_length;


% convert ideal waveform to freq. domain
range_profile_matrix = ifftshift( fft( fftshift(
  G_polar, 1 ), [], 1 ), 1 );
[g1,g2] = size(G_polar);
received_echo = zeros((g1+w1)-1,g2);
Match_Filter_response = zeros((((g1+w1)-1)+CR1)-1,g2);
% Match_Filter_response = zeros((((g1+w1)-1)+w1)-1,g2);
% waveform echo that enters the receiver

for n = 1:g2
    received_echo(:,n) = conv(
        range_profile_matrix(:,n), waveform );
    Match_Filter_response(:,n) = conv(
        received_echo(:,n),
        conj(flipud(Correlation_Ref)) );
end

[RE1,RE2] = size(received_echo);
[MF1,MF2] = size(Match_Filter_response);
adj_Match_Filter_response = zeros(MF1+2,MF2);
adj_Match_Filter_response(2:MF1+1,:)=
  Match_Filter_response;
[aMF1,aMF2] = size(adj_Match_Filter_response);
Int_Filter_response = zeros(code_length,g2);

for n = 1:sensor_props.code_length
    Int_Filter_response(:,:) = ...
adj_Match_Filter_response(n*code_length+1:(n+1)*code_length,:)+..
.
        Int_Filter_response(:,:);
end
 [IF1,IF2] = size(Int_Filter_response);
if  IF1 >= g1
    Int_Filter_response =
        Int_Filter_response(1:g1,1:g2);
else
    n = 0;
    IFL = IF1;
    while IF1 < g1
        n = n+1;
```

```
        adj_Int_Filter_response((n-
          1)*(IFL)+1:n*(IFL),:) =
          Int_Filter_response(1:(IFL),:);
        Int_Filter_response = adj_Int_Filter_response;
        [IF1,IF2] = size(Int_Filter_response);
    end
    Int_Filter_response =
        Int_Filter_response(1:g1,1:g2);
end
[IF1,IF2] = size(Int_Filter_response);
G_polar = ifftshift( ifft(
  fftshift(Int_Filter_response, 1 ), [], 1 ), 1 );
```

LIST OF REFERENCES

[1] W. G. Carrara, R. S. Goodman, and R. M. Majewski, *Spotlight Synthetic Aperture Radar, Signal Processing Algorithms*, Norwood, MA: Artech House, 1995.

[2] C. V. Jakowatz Jr., D. E. Wahl, P. H. Eichel, D. C. Ghiglia, and P. A. Thompson, *Spotlight-Mode Synthetic Aperture Radar: A Signal Processing Approach*, Norwell, MA: Kluwer Academic, 1996.

[3] L.J. Cutrona, W. E. Vivian and E. N. Leith, "A high-resolution radar combat surveillance system," *IRE Transactions on Military Electronics,* vol. MIL-5, no. 2, April 1961.

[4] S. W. McCandless Jr and C. R. Jackson, *SAR Marine User's Manual*, Washington, DC: U.S. Department of Commerce, 2004.

[5] M. Skolnik, *Introduction to Radar Systems*, 3rd ed., New York, NY: McGraw Hill, 2001.

[6] N. Levanon and E. Mozeson, *Radar Signals*, Hoboken, NJ: John Wiley & Sons, Inc., 2004.

[7] M. Skolnik, *Radar Handbook*, 3rd ed., New York, NY: McGraw-Hill, 2008.

[8] P. E. Pace, *Detecting and Classifying Low Probability of Intercept Radar*, 2nd ed., Norwood, MA: Artech House, 2009.

[9] E. Giusti and M Martorella, "Range Doppler and Image Autofocusing for FMCW Inverse Synthetic Aperture Radar," *IEEE Transactions on Aerospace and Electronic Systems*, vol. 47, no. 4, pp. 2807–2823, October 2011.

[10] D. Garren, P. Pace and R. Romero, "Phenomenology of low probability of intercept synthetic aperture radar via Frank codes," in *Proc. of SPIE, Algorithms for Synthetic Aperture Radar Imagery XXI*, Baltimore, 2014.

[11] D. A. Garren, P. E. Pace and R. A. Romero, "Use of P-3 coded transmission waveforms to generate synthetic aperture radar images," in *Proc. of the IEEE Radar Conference*, Cincinnati, Ohio, 2014.

[12] D. Lang, "Range sidelobe response from the use of polyphase signals in spotlight synthetic aperture radar," M.S. thesis, Dept. of Elec. Eng., Naval Postgraduate School, Monterey, CA, USA, 2015.

[13] Z. Wagner, D. Garren, P. Pace, "SAR imagery via frequency shift keying Costas coding," in *Proc. of the IEEE Radar Conference*, Seattle, WA 2017.

[14] D. C. Munson, Jr., J. D. O'Brien and W. K. Jenkins, "A tomographic formulation of spotlight-mode synthetic aperture radar," *Proceedings of the IEEE*, vol. 71, no. 8, pp. 917–925, 1983.

[15] J. L. H. Webb and D. C. Munson, Jr., "SAR image reconstruction for an arbitrary radar path," in *1995 International Conference on Acoustics, Speech, and Signal Processing*, May 1995.

[16] S. Xiao and D. C. Munson, Jr., "Spotlight-mode SAR imaging of a three-dimensional scene using spectral estimation techniques," *IEEE International Geoscience and Remote Sensing Symposium Proceedings,* 1998, vol. 2, pp. 642–644.

[17] M. Soumekh, *Synthetic Aperture Radar Signal Processing*, Hoboken, NJ: John Wiley & Sons, Inc., 1999.

[18] A. K. Jain, *Fundamentals of Digital Image Processing*, Englewood Cliffs, NJ: Prentice Hall, 1989.

[19] N. Touati, C. Tatkeu, A. Rivenq and T. Chonavel, "Phase coded Costas signals for ambiguity function improvement and grating lobes suppression," in *Vehicular Technology Conference*, 2013.

[20] J. Beard, "James K Beard's Complimentary Files," James K Beard, April 6, 2015. [Online]. Available: http://jameskbeard.com/jameskbeard/Files.html#CostasArrays

INITIAL DISTRIBUTION LIST

1. Defense Technical Information Center
   Ft. Belvoir, Virginia

2. Dudley Knox Library
   Naval Postgraduate School
   Monterey, California